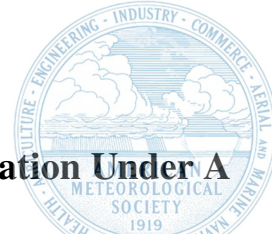




Generated using the official AMS L^AT_EX template v6.1



Stochastic Bifurcation of the North Atlantic Circulation Under A Mid-Range Future Climate Scenario With The NASA-GISS ModelE

Anastasia Romanou,^{a,b} David Rind,^a Jeff Jonas,^a Ron Miller,^a Maxwell Kelley,^a Gary Russell,^a
Clara Orbe,^a Larissa Nazarenko,^c Rebecca Latto,^b and Gavin A. Schmidt,^a

^a *NASA Goddard Institute for Space Studies, New York, NY.*

^b *Dept. of Applied Phys. and Applied Math., Columbia U., New York, NY.*

^c *Climate Systems Research, Columbia U., New York, NY.*

Corresponding author: Anastasia Romanou, anastasia.romanou@nasa.gov

Early Online Release: This preliminary version has been accepted for publication in *Journal of Climate*, may be fully cited, and has been assigned DOI 10.1175/JCLI-D-22-0536.1. The final typeset copyedited article will replace the EOR at the above DOI when it is published.

ABSTRACT: A 10-member ensemble simulation with the NASA GISS-E2-1-G climate model shows a clear bifurcation in the Atlantic Meridional Overturning Circulation (AMOC) strength under the SSP2-4.5 extended scenario. At 26°N, the bifurcation leads to 8 strong AMOC and 2 much weaker AMOC states, while at 48°N, it leads to 8 stable AMOC-on and 2 nearly AMOC-off states, the latter lasting approximately 800 years. A variety of fully coupled models have demonstrated tipping points in AMOC through hosing experiments, i.e. prescribing sufficient fresh water inputs in the subpolar North Atlantic. In the GISS simulations, there are no external fresh water perturbations. The bifurcation arises freely in the coupled system and is the result of stochastic variability (noise-induced bifurcation) associated with sea ice transport and melting in the Irminger Sea after a slowing of the GHG forcing. While the AMOC strength follows the near shut-down of the Labrador Sea deep convection initially, the Irminger Sea salinity and deep mixing determine the timing of the AMOC recovery or near collapse at 48°N, which varies widely across the ensemble members. Other feedbacks such as ice-albedo, ice-evaporation, E-P, and the overturning salt-advection feedback play a secondary role that may enhance or reduce the primary mechanism which is ice melt. We believe this is the first time that a coupled climate model has shown such a bifurcation across an initial condition ensemble and might imply that there is a chance for significant and prolonged AMOC slow down due to internal variability of the system.

SIGNIFICANCE STATEMENT: We believe this is the first time that divergent AMOC behavior has been reported for an ensemble of Earth System Model simulations using identical climate forcing and no prescribed fresh water perturbations. This response is a manifestation of noise-induced bifurcation, enhanced by feedbacks, revealing the role stochastic (or intrinsic) variability may play in AMOC stability.

1. Introduction

The Atlantic Meridional Overturning Circulation (AMOC) is a distinct pattern of the large-scale oceanic circulation, associated with northward transport of warm and salty waters and the concomitant release of heat to the atmosphere as this water cools and eventually subducts in the North Atlantic Subpolar Gyre and the Nordic Seas. Through this process, the AMOC regulates climate locally and regionally in the Northern hemisphere over seasonal, interannual and decadal scales, and globally over centennial scales (Buckley and Marshall 2016). At the same time, the AMOC is considered one of the tipping elements of the climate system (Lenton et al. 2008), with low probability of a collapse occurring in the 21st Century but with high impact, according to the latest two Assessment Reports (AR5 and AR6) of the Intergovernmental Panel on Climate Change (IPCC) (Stocker et al. 2013; Masson-Delmotte et al. 2021).

This paper investigates the AMOC bistability in the GISS-E2-1-G model simulations under surface warming conditions consistent with middle-of-the-road projections of anthropogenic greenhouse gas (GHG) emissions, prescribed in the SSP2-4.5 projection. In a 10-member ensemble scenario, the overturning circulation at 48°N in the Atlantic nearly collapses (reaches 0.7 ± 0.05 Sv over the course of approximately 400 years) in 2 members and recovers in the rest at different times (Fig. 1). Eventually, the AMOC of those two ensemble members will recover after 800 years of simulations (see SMFig. 1 in the Supplementary Material).

The possibility that the AMOC can have multiple equilibrium states and how it may transition between them has been a central theme of AMOC stability analyses since the 1960s (Stommel 1961; Bryan 1986; Manabe and Stouffer 1988; Rahmstorf 1996; de Vries and Weber 2005; Drijfhout et al. 2011; Jackson and Wood 2018; Weijer et al. 2020; Hirschi et al. 2020). Observations of the fresh water flux into the Atlantic basin based on ship data and ARGO floats may suggest that the present-day North Atlantic ocean is in a bi-stable regime (Bryden 2011; Garzoli et al. 2013);

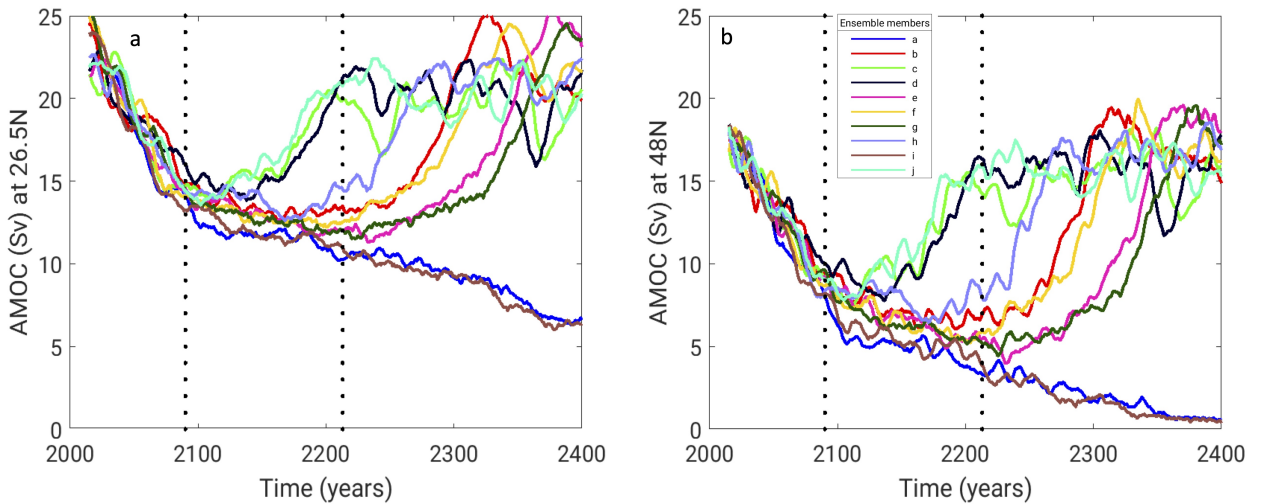


FIG. 1. AMOC strength, defined as the maximum overturning streamfunction below 500m, at (a) 26.5°N and (b) at 48°N , from 10 ensemble members of the SSP2-4.5 scenario simulation. Vertical dotted lines correspond to times of change in GHG forcing (see Fig. 2a). All fields are smoothed using a 10-year moving average filter.

characterized by a possible stable AMOC-on and a possible AMOC-off state, but the timing and the conditions for any transition, as well as whether we are currently in a weak AMOC state remain highly uncertain (Caesar et al. 2021; Kilbourne et al. 2022). Transition to a stable AMOC-off state, which may be long-lasting but not necessarily permanent, could have unknown environmental and societal consequences, and therefore this issue is of critical importance to science and humanity.

The paleoclimate record contains crucial evidence of abrupt or gradual transitions in AMOC strength that may be relevant for our future climate (e.g., Jansen et al. (2018); Thornalley et al. (2018); Schmidt and LeGrande (2005)). For example, AMOC bi-stability has been proposed as a mechanism that explains rapid climate variability between glacial and interglacial periods in the Pleistocene (Lynch-Stieglitz 2017; Moffa-Sánchez et al. 2019), and in the Holocene, derived from ice-core records (Dansgaard et al. 1993; Blunier and Brook 2001) or sediment cores (de Abreu et al. 2003). In Most climate models, regardless of the greenhouse gas (GHG) forcing scenario, predict a moderate slowdown (up to 12 Sv), but not a complete shutdown of the AMOC in the 21st Century (Weijer et al. 2020). This suggests that these models are in mono-stable AMOC regime, at least within the 21st Century. Bi-stability in models was initially explored using a fresh water flux in the form of a “hosing” perturbation imposed over the North Atlantic, for example in box models (Rahmstorf 1996), in non-eddy permitting models with a flux adjustment (Stouffer et al.

2006; Hawkins et al. 2011; Hu et al. 2012; Sijp et al. 2012), or in non-eddy permitting models without flux adjustment (Rind et al. 2001; Drijfhout et al. 2011).

A main mechanism that controls the AMOC stability relates to the salt-advection feedback (Drijfhout et al. 2011). A positive salt-advection feedback implies that a weakening AMOC will transport less salt into the Atlantic that leads to freshening there, lower surface density, further obstructing convection and eventually further weakening of the AMOC. A potential metric (also known as an indicator or fingerprint or predictor) of the salt-advection feedback is either the fresh water transport via the overturning circulation (denoted as “ M_{ov} ”) evaluated either across the South Atlantic subtropical gyre, e.g. across latitude 33°S (de Vries and Weber 2005; Castellana and Dijkstra 2020; Li et al. 2021), or the divergence of the fresh water transport via the overturning circulation between the South Atlantic gyre and the Arctic Ocean (Huisman et al. 2010; Liu et al. 2017). A positive M_{ov} implies that the AMOC imports fresh water into the Atlantic and in case of AMOC weakening such a fresh water import would be reduced, leading to salinification of the Atlantic and strengthening of the convection and the AMOC, i.e. a stable AMOC-on state (negative salt-advection feedback). Conversely, a negative M_{ov} exports fresh water from the Atlantic, therefore in case of AMOC weakening, the fresh water export would be reduced, which would further freshen the basin and promote further AMOC weakening (positive salt-advection feedback). In general, low-resolution climate models exhibit a positive M_{ov} (Weaver et al. 2012; Mecking et al. 2017), and thus predict a mono-stable AMOC instead (i.e. no AMOC-off state). In higher resolution, eddy-permitting models, the AMOC-related northward transport of fresh water is increased due to eddies and less-diffusive ocean currents, compared to lower resolution models. These models can exhibit a stable AMOC-off state (Mecking et al. 2016). Nonetheless, model biases can be critical for determining which state is obtained (Liu et al. 2017).

Meanwhile, there is a growing number of studies suggesting that M_{ov} is not a good indicator of AMOC stability (see Sgubin et al. (2015); Rind et al. (2018); Gent (2018); Castellana and Dijkstra (2020) and Weijer et al. (2019) for a detailed discussion). Instead, other feedbacks within the North Atlantic play a role, opposing or reinforcing the salt-advection feedback. With specific attention to coupled climate models, where such feedbacks are not damped, as opposed to standalone ocean models which are forced with prescribed variability in the atmosphere and sea ice, it has been

reported that atmospheric and land/sea ice feedbacks may play a significant role (Weijer et al. 2019).

The AMOC decline under increasing GHG forcing is associated with the development of a “warming hole”, i.e., the lack (or delay) of the warming over the North Atlantic subpolar gyre (Menary and Wood 2018) due to the reduced northward heat transport by the AMOC. Such a localized cooling would promote deep convection, therefore acting as a negative feedback to the AMOC weakening. On the other hand, an atmospheric-temperature feedback ensues then because of the colder air (and sea surface) temperatures associated with the warming hole. Colder air holds less moisture and together with the reduced SSTs results in reduced evaporation, i.e. freshening of the subpolar gyre (SPG), acting as a positive feedback to the AMOC decline (Rind et al. (2018)). Another atmospheric feedback arises with the southward shift in the Atlantic Intertropical Convergence Zone (ITCZ) that follows the AMOC weakening and leads to less precipitation over the northern subtropics and thus a salinification there. These positive anomalies are then transported northward to the SPG and help reinvigorate the AMOC (negative feedback to AMOC weakening, Jackson and Wood (2018)).

Furthermore, sea ice melting leads to a weakening of the AMOC (Li et al. 2021) due to large fresh anomalies that spread from the Arctic Ocean into the SPG and which further weaken AMOC. At the same time sea ice reductions lead to albedo reductions and intense heat losses which promote convection and strengthen the AMOC. Conversely, if sea ice extends or is transported into the region of the warming hole, it might grow further, preventing air-sea exchanges and AMOC strengthening (positive feedback to AMOC weakening).

It is therefore clear that in coupled climate models, where all these different feedbacks (and maybe others) are at play, given each particular model’s biases and missing processes, the relative role of each feedback to the salt-advection feedback as well as the relative role of the internal variability to the forced response, i.e. the stochasticity of the modeled climate, may make the transition to an AMOC-off state possible regardless of the M_{ov} metric.

In the previous generation of the GISS coupled climate model (GISS-E2-R, Rind et al. (2018)), one simulation with abrupt 4xCO₂ forcing and another with interactive aerosols exhibited a bi-stable state that was also obtained without any external perturbation in the fresh water forcing. In that simulation, the collapse was attributed to cooling in the North Atlantic associated with

the aerosol direct effect on cloud cover and thus planetary albedo; by providing local cooling in the midst of an otherwise warming climate, evaporation was decreased relative to precipitation, resulting in freshening. The recovery was associated with continued global warming spreading poleward from low latitudes and downward, ultimately reducing the vertical stability from below at high northern latitudes, allowing overturning to resume.

While several coupled climate, as well as uncoupled, ocean modeling studies have shown that there is a tipping point where sufficient forcing (e.g. by fresh water addition) can shut down the AMOC, here we show that individual members of an ensemble of ten coupled runs with the GISS E2.1-G model forced with the SSP2-4.5 scenario, exhibit contrasting AMOC responses, with some showing near collapse (AMOC-off) for at least 800 years, at 48°N, while others recover to current climate levels (AMOC-on).

The objective of this paper is to first explain how the bi-stability establishes itself and then place this result, which is unique in that the bi-stability arises within a single forcing scenario of the same model and without the aid of externally imposed “hosing” or prescribed feedback, in the context of other studies of AMOC stability. This leads to an interesting question of whether such a bifurcation in AMOC stability can arise in Nature, given especially that we suspect Nature is already in a bi-stable state and a transitory period of weakened strength. Could the AMOC-off state arise in a similar way as in our model?

The paper is organized as follows: in Section 2 we provide some information on the model configuration, the ensemble simulations, and methods we use in the analysis, e.g. the regional salinity budget and the deep mixing volume. In Section 3 we discuss SPG cooling and mixing and then describe the results of the salinity budget analysis in the Labrador and Irminger Sea basins, and consider the forced response vs. the intrinsic variability. We describe the sea ice and relevant atmospheric and oceanic feedbacks that contribute to the persistent AMOC near-shutdown at 48°N in two of the ensemble members and the mechanism of recovery for the rest of the ensemble. Lastly, in Section 4, we offer a discussion on the GISS-E2-1 model skill and place our analysis into context with stability work of modern and paleoclimate analogs.

2. Methods, Models, Data

a. Model configuration and simulations

We analyze the AMOC response to the Shared Socioeconomic Pathway (SSP) 2-4.5 (Meinshausen et al. 2019) greenhouse gas (GHG) emissions and mitigation scenario, in the NASA Goddard Institute for Space Studies (GISS) version E2.1 climate model (GISS-E2-1-G). These simulations were part of the official submission of the NASA GISS climate group to the Climate Model Intercomparison Project phase 6 (CMIP6) (Eyring et al. 2016).

The atmospheric component of GISS ModelE has 2° by 2.5° latitude and longitude resolution respectively, 40 vertical layers and a model top at 0.1 hPa. The ocean component, GISS Ocean v1, is mass conserving with a free surface, natural surface boundary conditions for heat and fresh water fluxes (Russell et al. 1995), horizontal resolution of 1° by 1.25° in latitude and longitude respectively and 40 vertical layers (Kelley et al. 2020). The GISS Ocean v1 model has 5 to 20 m resolution in the seasonal mixed layer, 20 to 80 m resolution in the thermocline and 100–200 m at depths greater than 1000 m. Heat, salt, and tracers are advected by the quadratic upstream scheme (Prather 1986) and are vertically mixed by the K-profile parameterization (KPP, Large et al. (1994)). Eddy related fluxes by mesoscale baroclinic turbulence are parameterized following the Gent-McWilliams parameterization (GM, Gent et al. (1995)) with variable coefficients (Kelley et al. 2020) where mesoscale transport is expressed in local quasi-isopycnal layering, and the vertical diffusivity includes a contribution from tidal dissipation which mostly impacts the shallow water regions bordering the North Atlantic. Ventilation of marginal seas has been increased by slight tuning of the strait depths and by increased horizontal diffusivity locally. Previous sensitivity studies (Marshall et al. 2017; Romanou et al. 2017) showed good agreement with observations with regards to uptake of passive tracers.

The sea ice component has two mass layers and two thermal layers in each mass layer. The sea ice dynamics is based on a formulation of the viscous-plastic rheology (Zhang and Rothrock 2000) and the sea ice thermodynamics uses the “brine-pocket” parameterization (Bitz and Lipscomb 1999; Schmidt et al. 2004) that allows salt to play a more active role in the specific heat and melt rates of sea ice. Processes relevant to the salt budget (e.g., gravity drainage and flushing of meltwater) are consistently treated with the brine pocket physics.

Land ice has an upper layer 0.1 m thick and evenly distributed variable amount of snow, and a lower layer 2.9 m thick. If snow exceeds 91.6 kg/m^2 , 10% is compacted into ice, while if surface heating melts the upper layer ice, melt-water is directed into the ocean. The purpose of this complexity is to approximately conserve ocean mass and ensure long-term stability of ice sheet mass. Each year one tenth of the iceberg arrays, distributed over the source time steps, are deposited into specific ocean cells, mainly near southern Greenland and low-lying Antarctica (SMFig. 2).

Comprehensive reviews of the model physics, historical and future climate change simulations are provided in Kelley et al. (2020); Miller et al. (2021); Nazarenko and co authors (2022).

b. The SSP2-4.5 ensemble simulations

The nominal radiative forcing for SSP2-4.5 represents a “middle-of-the-road” scenario that continues the forcing patterns of the late-historical simulation after year 2014 in terms of anthropogenic emissions and developments in environmental systems (Fig. 2a).

Each of the 10 ensemble member simulations for the historical period and SSP2-4.5 continuation were initialized from the pre-industrial control run at 20-year increments (Miller et al. 2021). The pre-industrial control run itself was spun up for about 7500 years.

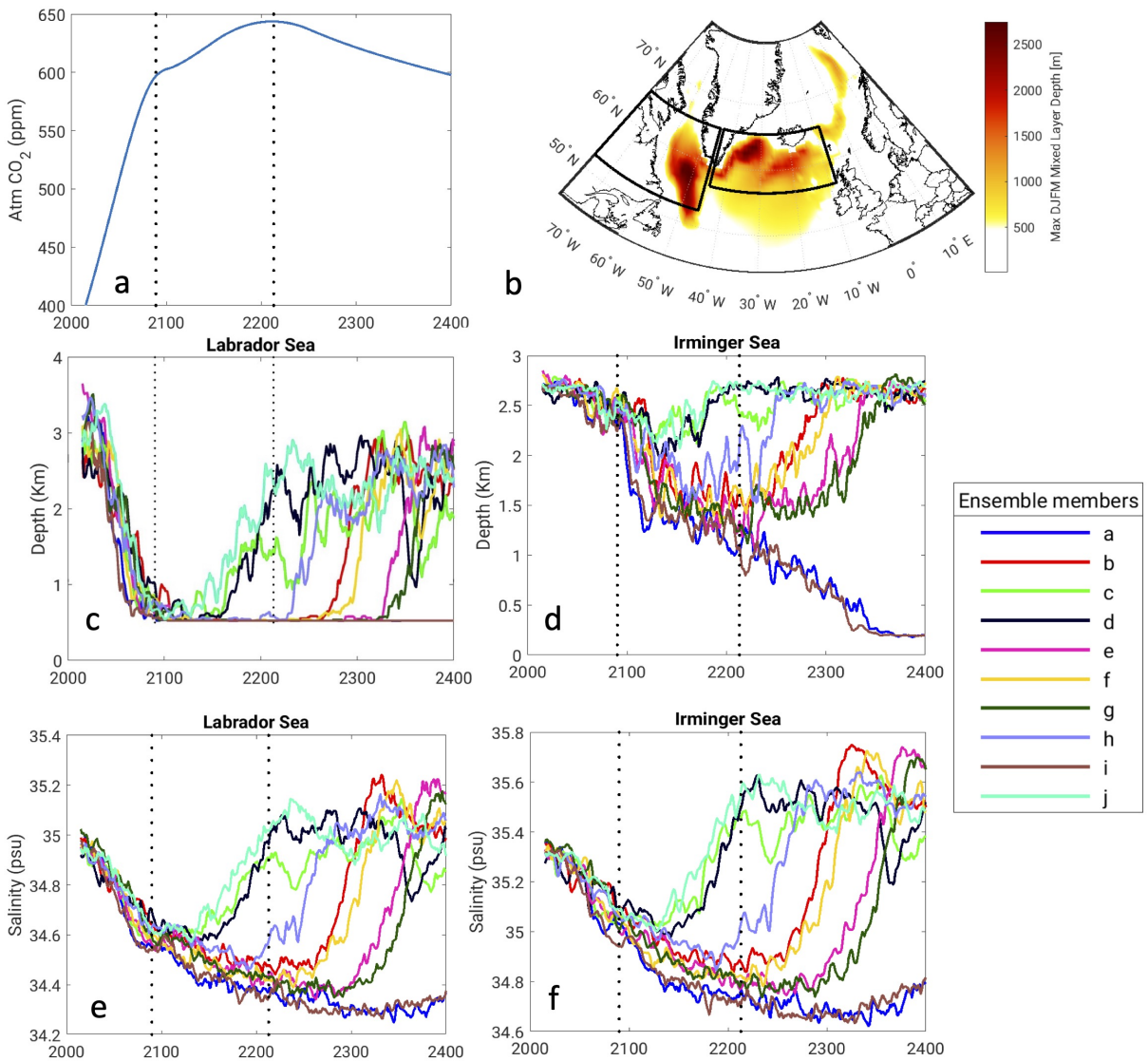


FIG. 2. a) Atmospheric CO₂ concentration pathway as prescribed in the SSP2-4.5 forcing scenario. Vertical dotted lines correspond to times of change in the GHG forcing rate. b) Ensemble mean, winter maximum mixed layer depths (MLDs) in the SSP2-4.5 simulation with the GISS-E2-1-G model; MLDs are defined as the maximum depths over the December-January-February-March period 2015-2020. Black boxes indicate areas involved in salinity budget analysis in sections 3.c.1 and 3.c.2: Labrador: 52.5-65.5°N; 75.6-45.6°W Irminger: 56.5-65.5°N; 44.4-10.6°W. Maximum regional, monthly DJFM mixed layer depths (m) in each ensemble member in the Labrador (c) and Irminger Sea (d). Average upper 1000m mean DJFM salinity (psu) in the Labrador (e) and Irminger Sea (f). Vertical dotted lines correspond to times of change in GHG forcing (see Fig. 2a). All fields are smoothed using a 10-year moving average filter.

c. Deep mixing volume (DMV)

North Atlantic mixed layer depths (MLDs) in the subpolar gyre (SPG) (Fig. 2b) are considered good indicators of deep water mass formation and link to the AMOC strength (Spall 2004). To estimate the rate of formation of dense waters in the regions denoted in Fig. 2b we use two different methods:

- 1) the December-January-February-March (DJFM) monthly and regional maximum mixed layer depth (MLD) (Figs. 2c,d and SMFig. 3), following Schott et al. (2009); Yashayaev and Loder (2009) and
- 2) the deep mixed volume (DMV) method (Brodeau and Koenigk 2016) which is defined as the integrated volume of all the grid cells where the DJFM convective mixing extends below 1000 m for a period of 1 year, and has units of Sverdrups (SMFig. 4).

The MLDs in the model are diagnosed following the CMIP6 protocols (mlotst), as the depth where σ_θ differs from that at 10 m depth by more than 0.125 kgm^{-3} . A comparative analysis of DMV in CMIP6 models (including GISS-E2-1-G) is offered in Heuzé (2021).

d. Salinity budgets

Several studies have pointed out the dominant role that the subpolar fresh water fluxes play in the AMOC variability (Kuznetsova and Bashmachnikov 2021) and its high meridional coherence on decadal and longer time scales (McCarthy et al. 2015).

To assess the fresh water budgets in the Labrador and Irminger Seas, we will follow the approach described in Ren and Riser (2009) that estimates the salinity budget in terms of the horizontal advection convergence, vertical diffusion and entrainment, and fresh water inputs from the surface, i.e evaporation, precipitation, sea ice formation, land-ice (glacial) melt, sea ice melt and riverine outflow (for details see Appendix).

Furthermore, in order to assess the large scale salt-advection feedback in the Atlantic, we estimate the magnitude of the fresh water transport at a South Atlantic subtropical gyre section (33°S) and other latitudes in the North Atlantic and the Arctic Ocean as is typically done in AMOC stability studies (e.g. de Vries and Weber (2005); Lobelle et al. (2022), see Appendix).

TABLE 1. SSP2-4.5: Winter (DJFM) surface air temperature (deg C), decadal change from 2015-2024 average

Run	YR 2050*	YR 2090	YR 2200	YR 2300
	Avg atmCO ₂ 507 ppm	598 ppm	643 ppm	621 ppm
	Glb(Lab, Irm)	Glb(Lab, Irm)	Glb(Lab, Irm)	Glb(Lab, Irm)
<i>a</i>	0.9 (1.6, 0.7)	1.5 (2.2,-0.4)	1.7 (1.2,-3.7)	1.4 (-0.2,-5.7)
<i>b</i>	1.1 (0.4, 0.2)	1.7 (1.5, 0.1)	2.0 (1.7,-1.9)	2.2 (3.4, 2.2)
<i>c</i>	1.0 (0.6, 1.0)	1.5 (0.8, 0.1)	2.2 (2.6, 1.5)	2.2 (4.2, 2.5)
<i>d</i>	1.0 (1.7, 0.9)	1.7 (2.2, 0.2)	2.3 (4.3, 2.2)	2.3 (5.1, 3.4)
<i>e</i>	0.9 (2.9, 1.2)	1.5 (1.8,-0.8)	1.7 (2.9,-2.8)	1.8 (2.9,-1.2)
<i>f</i>	1.0 (1.5, 0.3)	1.6 (2.0,-0.4)	1.8 (1.7,-2.2)	2.1 (3.0, 0.9)
<i>g</i>	0.9 (-0.0, 0.3)	1.5 (1.3,-0.1)	1.7 (1.0,-2.1)	1.8 (1.2,-1.7)
<i>h</i>	0.9 (1.0, 0.1)	1.6 (1.9, 0.1)	1.9 (2.5,-1.1)	2.3 (5.0, 3.0)
<i>i</i>	0.9 (1.1, 0.3)	1.5 (1.3,-0.8)	1.6 (1.1,-4.3)	1.4 (-1.2,-6.7)
<i>j</i>	1.0 (1.5, 0.7)	1.6 (2.0, 0.1)	2.4 (4.9, 2.7)	2.1 (4.3, 2.6)
mean	0.99(1.24,0.58)	1.57(1.70,-0.20)	1.93(2.40,-1.17)	1.96(2.76,-0.08)
std	0.08(0.82,0.37)	0.09(0.44,0.38)	0.27(1.35,2.47)	0.35(2.15,3.66)

*Decadal averages centered in year shown.

3. Results

a. Subpolar gyre surface cooling

While wintertime (DJFM) global mean surface air temperatures (Table 1) and sea surface temperatures (SSTs, SMFig. 5) do not differ much initially among ensemble members, in the 2050s Labrador Sea air temperatures exhibit large inter-ensemble spread, with some members being significantly warmer than the ensemble mean. The Irminger Sea temperature changes are generally colder and the spread is smaller than in the Labrador Sea, consistent with the development of the warming hole. By the 2090s, the global mean temperatures still differ little among ensemble members. Meanwhile, temperature anomalies in the Irminger Sea are now substantially more negative than in the Labrador Sea. By 2200, Irminger Sea temperatures have further decreased in most of the members (evidence of a deepening warming hole), especially more so in runs *a* and *i*, while members *c,d* and *j* have warmed up sufficiently to converge with the Labrador and global mean temperatures. By 2300, members *a* and *i* are substantially colder than the rest. However, temperatures in SPG are not found to be a good predictor of the AMOC recovery, as some runs that have a more prominent warming hole (i.e. colder air and sea surface temperatures) recover faster (e.g. member *f* vs *g*) while others do not. Additionally, SMFig. 5 shows that AMOC recovery leads the contraction of the warming hole in the Labrador and Irminger Seas.

b. Subpolar gyre deep mixing

Deep convection in the Labrador, Irminger and Greenland-Iceland Seas has long been linked to AMOC variability (Talley et al. 2003). Some studies highlight the primary role of the Labrador Sea (Rhein et al. 2011; Talley et al. 2003) while others dispute it (Pickart and Spall 2007). Recent observational and modeling work points more to the importance of the Irminger Sea and the Greenland-Iceland Seas (Lozier et al. 2019; Petit et al. 2020).

In the GISS-E2-1-G, the correlation between the AMOC strength at 48°N and at 26°N (Fig. 1a,b respectively) in each ensemble member, averaged over all the ensemble members is high: 0.97 ± 0.02 (we apply a low pass filter of all periods less than 1 year). Similarly the mean correlation between the AMOC strength at 48°N and the MLD in the Labrador and Irminger Seas is 0.90 ± 0.05 and 0.90 ± 0.06 respectively. The correlation between the AMOC strength at 48°N and the deep mixing volume (DMV) in the Labrador and the Irminger Sea averaged over all ensemble members is 0.86 ± 0.06 and 0.91 ± 0.07 respectively. Such high correlations suggest that the AMOC variability in the SSP2-4.5 ensemble is linked to processes in the subpolar gyre (SPG) that control convective mixing and dense water formation in the Labrador and Irminger Seas.

Initially, Labrador Sea (LS) convection extends to more than 3000 m (Fig. 2c) and produces deep mixed volumes that exceed 25 Sv (SMFig. 4a). By 2090, LS convection barely reaches 500 m depth and does not contribute DMV in any of the simulations. In the four centuries after 2090, LS convection recovery in all but two ensemble members, lags the recovery of the AMOC at 48°N by periods that vary between 5 and 200 years (Fig. 1b, 2c, SMFig. 4a and SMFig. 6), implying that the Labrador Sea convection is not driving the AMOC recovery.

Irminger Sea convection, on the other hand, which extends initially to 2800 m (Fig. 2d) and produces deep mixing volumes of about 15 Sv (SMFig. 4b), declines in all members during the twenty-first and twenty-second Centuries. It continues to decline in two of the ensemble members (a and i) beyond the 2200s. The remaining eight members maintain mixed layers extending below 1500 m that eventually recover to their present-day values during the next few centuries (see also SMFig. 6). In these ensemble members deep convection is reinvigorated at the same time as the recovery of the AMOC at 48°N. For each ensemble member, the timing of the restoration of the deep mixing in the Irminger Sea precedes that of the restoration in the Labrador Sea, suggesting that the Irminger Sea determines the AMOC recovery (SMFig. 6).

Other basins which observations suggest contribute to North Atlantic Deep Water (Lozier et al. 2017) and thus the AMOC, such as the Scotland-Iceland basin and the Greenland-Iceland-Norway (GIN) Sea, in GISS-E2-1-G develop convection that extends below 1000 m in most ensemble members but produce little volume of deep water (SMFig. 3 and SMFig. 4c,d). Specifically, there is no contribution to dense waters in the North Atlantic through the Iceland-Faroe Islands sills. It is therefore the behavior of the Irminger Sea that controls whether AMOC at 48°N will nearly shut down or recover in each ensemble member after 2100.

Since SST evolution does not help explain the AMOC bifurcation in the ensemble members (SMFig. 5), to further investigate the causes of the changing MLDs in these regions we turn to upper ocean salinity budget changes in the LS and IS basins (Fig. 2e and f).

c. Subpolar gyre salinity budgets

In the following sections, we show figures only for ensemble members c, g and i, which exhibit different AMOC responses after 2100: the AMOC of member c recovers within 10 years after the forcing begins to slow down, the AMOC of member g remains weak for several decades but eventually recovers, while the AMOC of member i continues to decline and eventually nearly collapses (although after 800 years it also recovers). Results for the full suite of ensemble members are included in the Appendix (SMFigs. 7-12). We also focus on AMOC at 48°N unless otherwise noted.

1) LABRADOR SEA

During the period 2015-2090, when the SSP2-4.5 forcing increases rapidly, the Labrador Sea (LS) region freshens reaching a maximum freshening around 2050 (Fig. 3a). During 2090–2200, when the SSP2-4.5 forcing slows, ensemble member c tends to salinify but exhibits large decadal variability in salinity, while members g and i continue to freshen at a constant rate. After 2200, both run i shows constant freshening but run g shows large salinification after 2300. Note that the AMOC strength in run g starts to recover after 2200 (Fig. 1a,b). The behavior of these three ensemble members is representative of the entire group; some runs behave like c (namely, runs d, j), while run a behaves like run i and the rest of the runs behave like run g, where the AMOC strength declines but eventually recovers at very different time periods (SMFig. 7).

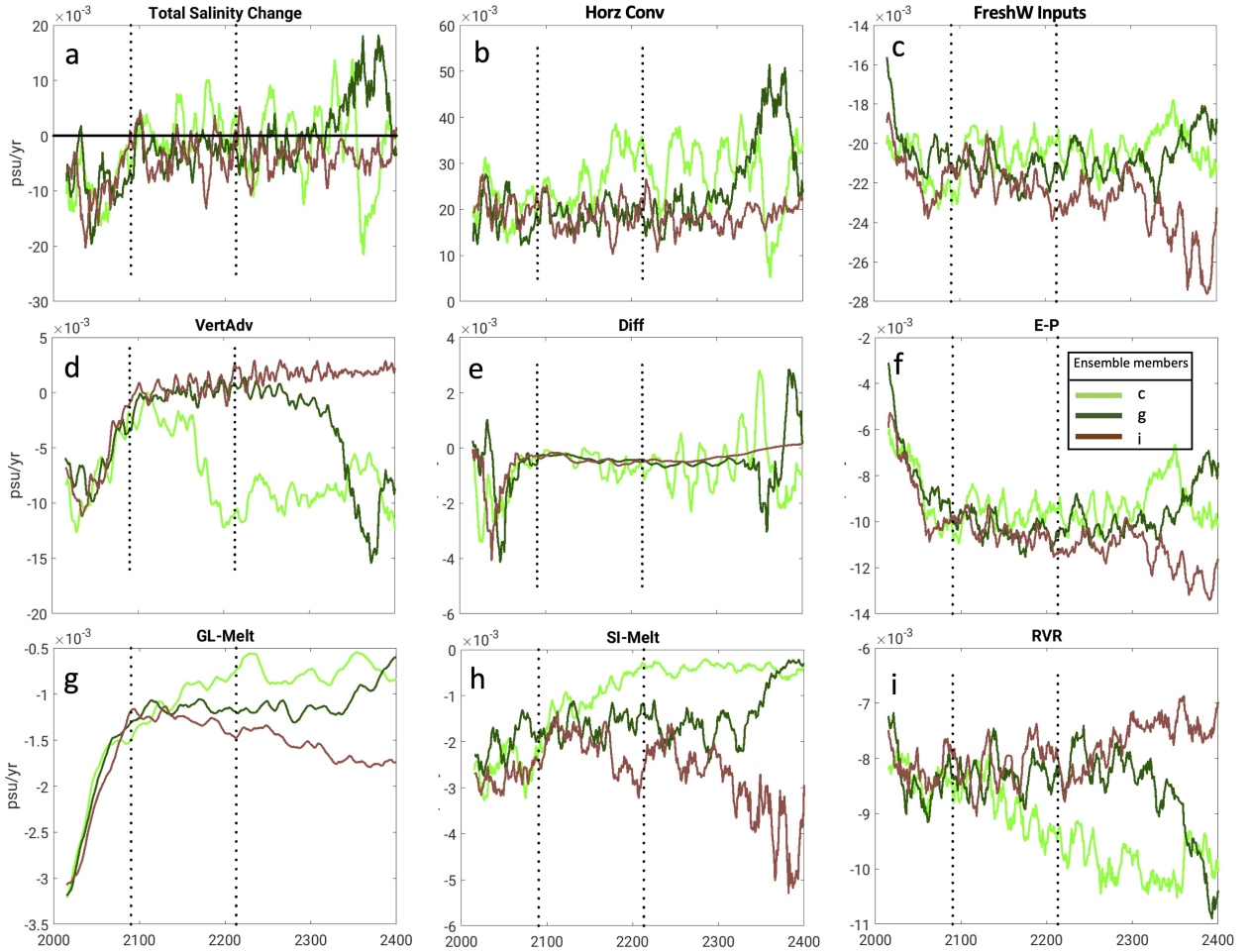


FIG. 3. Net salinity tendency and individual salinity budget terms in the **Labrador Sea** (psu/yr) for ensemble members c (light green line), g (dark green line) and i (brown line). Color-scheme corresponds to Figs. 1a,b. (a) Net salinity budget change in the top 1000 m, (b) salinity change due to horizontal transport convergence, (c) salinity change due to fresh water inputs, (d) salinity change due to entrainment at 1000 m, and (e) salinity change due to vertical diffusion at 1000 m. The surface fresh water tendency term (panel c) is further decomposed to (f) salinity change due to E-P, (g) salinity change due to glacial (or land) melt, (h) salinity change due to sea ice melt and (i) salinity change due to riverine inputs. Positive (negative) values indicate increase (decrease) in area averaged salinity. All timeseries are smoothed with a 10-year moving average filter. Vertical dotted lines correspond to times of change in GHG forcing (see Fig. 2a). Salinity budget terms for all the ensemble members are shown SMFig. 7.

Breaking down the salinity contributions from each of the terms in Eq. 5 (see Appendix), we see that during the 21st Century, the freshening in all the simulations is mainly due to increasing fresh

water inputs from the surface (Fig. 3c), aided by entrainment (Fig. 3d) and diffusive mixing (Fig. 3e) at the bottom of the mixed layer, all of which tend to overpower the salinification induced by the horizontal transport convergence (Fig. 3b). Generally, in all the ensemble members (SMFig. 8), changes in the horizontal transport convergence are primarily due to changes in the transports through the southern and eastern boundary which tend to salinify and slightly freshen the region respectively (Fig. 2e,f). Freshwater inputs from the surface, mainly E-P and rivers (Figs. 3f,i and SMFig. 9), generally increase leading to more freshening. Glacial and sea ice melt decrease with time in all the simulations in a similar fashion. These changes in the fresh water inputs are enough to cancel out horizontal transport convergence in run c, but in g and i are slightly larger leading to net freshening.

From 2090 to 2200, in ensemble member c, freshening via entrainment at 1000 m depth and freshwater inputs at the surface is not able to counteract the salinification through horizontal convergence (Fig. 3b,c,d). Hence in this simulation, deep convective mixing in LS recovers early (Figs. 2c and SMFig. 3a) and therefore AMOC recovers as well (Fig. 1a,b). In ensemble members g and i, however, salinification due to horizontal transport convergence is weaker, especially via the eastern boundary (SMFig. 8), than the freshening through the surface inputs while entrainment and diffusion are almost zero.

After 2200, salinification by horizontal transport convergence in run c is steady but with large decadal variability and slightly exceeds the surface freshening, entrainment and diffusive mixing from below. In run g, horizontal transport convergence increases progressively after 2300, again due to the eastern boundary transport, and eventually overcomes the freshening imposed by the other terms. In run i, the horizontal transport convergence continues to weaken and is unable to surpass the freshening due to fresh water inputs from the surface. Again, the eastern boundary transport leads to continuously more freshening in the region and the southern boundary transport leads to more salinification. E-P and riverine inputs stabilize after 2090 until approximately 2300 (Fig. 3f,g,h,i) in run c and g while E-P further increases in run i, leading to more freshening. Glacial and sea ice melt decline substantially in run c but stabilize in run g and further increase in run i, leading to more freshening in the latter.

In conclusion, in the Labrador Sea, salinification via horizontal transport across the eastern boundary is too weak to counteract surface freshening in all but the three ensemble members with

early AMOC recovery. To examine what controls the AMOC recovery in the remaining seven ensemble members we look at the salt budget in the other main convection region in our model, the Irminger Sea.

2) IRMINGER SEA

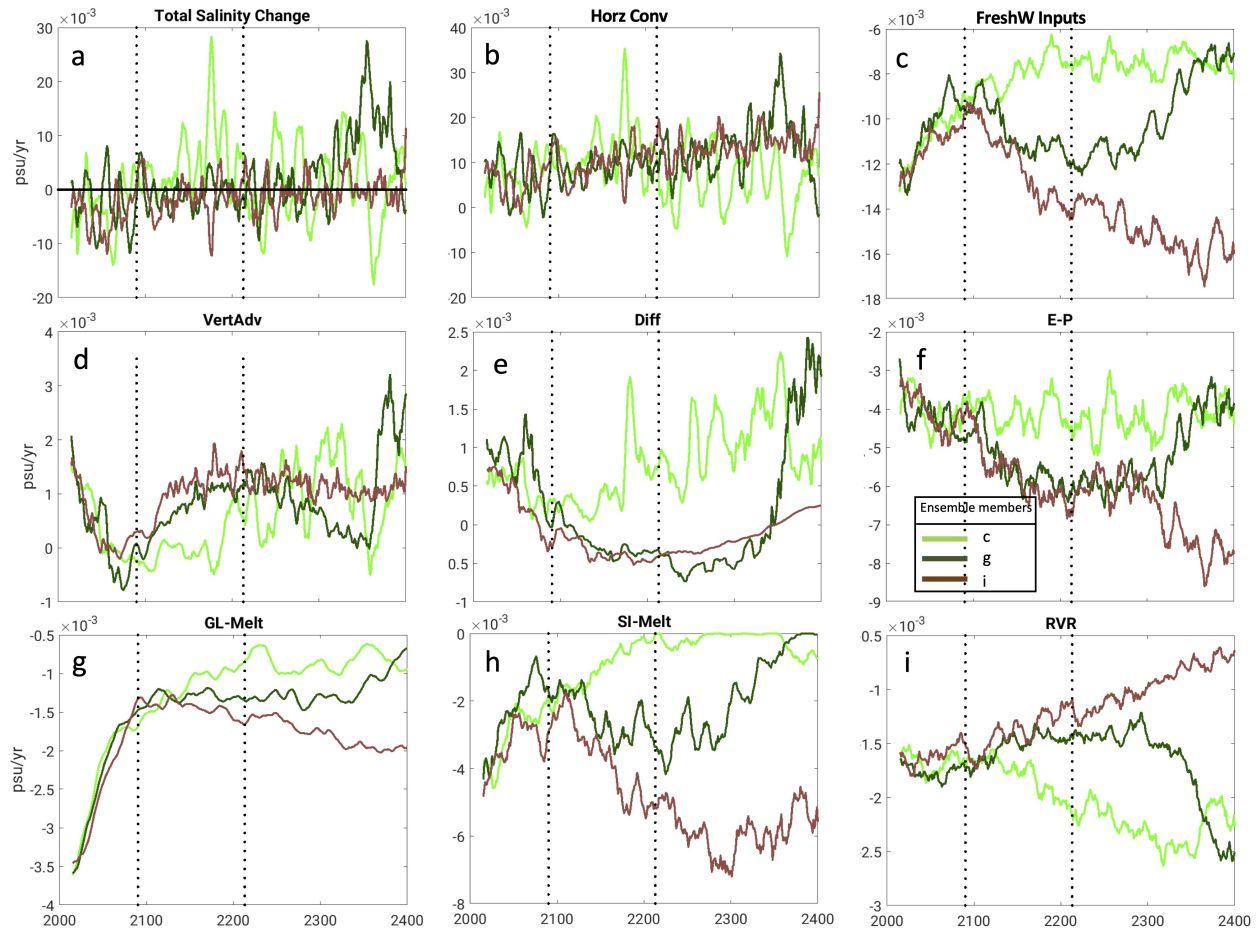


FIG. 4. Net salinity tendency and individual salinity budget terms in the **Irminger Sea** for ensemble members c, g and i, as in Fig. 3. Positive (negative) values indicate increase (decrease) in area averaged salinity. Vertical dotted lines correspond to times of change in GHG forcing (see Fig. 2a). Salinity budget terms for all the ensemble members is shown in SMFig. 10.

In the 21st Century, the Irminger Sea (IS) maintains most of its deep mixing and deep water formation (Fig. 2d and SMFig. 4b). During that period, the IS experiences an average freshening (Fig. 4a) in all the ensemble members because salinification due to vertical advection and diffusion

declines (Fig. 4d,e), while salinification due to horizontal convergence remains constant (Fig. 4b) but is eventually overcome by the freshening provided by surface fresh water inputs (Fig. 4c and SMFig. 10) even though they also decline with time.

In contrast to the LS, where fresh water inputs through the surface increase with time during this period, in IS they tend to decrease (Fig. 3c vs. Fig. 4c, also see SMFig. 10). Transports in the IS region lead to salinification via the western boundary and less so via the southern boundary, and freshening via the northern boundary (SMFig. 11). (Note that the IS western boundary is shorter than the LS eastern boundary, and its southernmost section contributes to the salinification of IS). Freshening due to surface fresh water inputs is similar in all runs during 2015-2090 (Fig. 4c and SMFig. 11), with the glacial and sea ice melt being as important as E-P, although the melt magnitude decreases with time while E-P increases. River input changes are small (Fig. 4f,g,h,i). It is important to note that the relative contribution of the ice melt compared to that from E-P and rivers in the Irminger Sea salinity is significantly higher than in the Labrador Sea (SMFig. 9 vs. SMFig. 12).

After 2090 and at least till 2300, ensemble member c exhibits larger decadal variability in salinity change (Fig. 4a) than ensemble members g and i which have weakened AMOC and weakened northward transport of warm and salty subtropical water. Horizontal transport convergence salinifies the domain in all three runs by a similar magnitude (Fig. 4b), while surface fluxes lead to increased freshening (Fig. 4c) in runs g and i and a sustained decrease in run c. This is important as it shows that advective criteria only become important after 2300 in run g, well after the AMOC has started slowly increasing, which occurs after 2210. In run c, the transport induced salinification originates from the western boundary and overcomes the freshening through the northern boundary (SMFig. 11) while in runs g and i both the east and the western boundary transports lead to salinification, and the southern boundary transport is nearly shut down. In run g, transport through the southern and eastern boundaries starts to increase leading to salinification of the IS after 2250 and 2300 respectively.

Freshening from surface fluxes (Fig. 4c and SMFig. 12) in run g continues after 2150 until about 2250 and then slowly decreases in magnitude, coincident with the slow recovery of the AMOC. In run i however, surface freshening increases steadily after 2100 (Fig. 4c), driven by sea ice and to a lesser extent glacial ice melt (Fig. 4g and h). and E-P (Fig. 4f). The relative importance of the

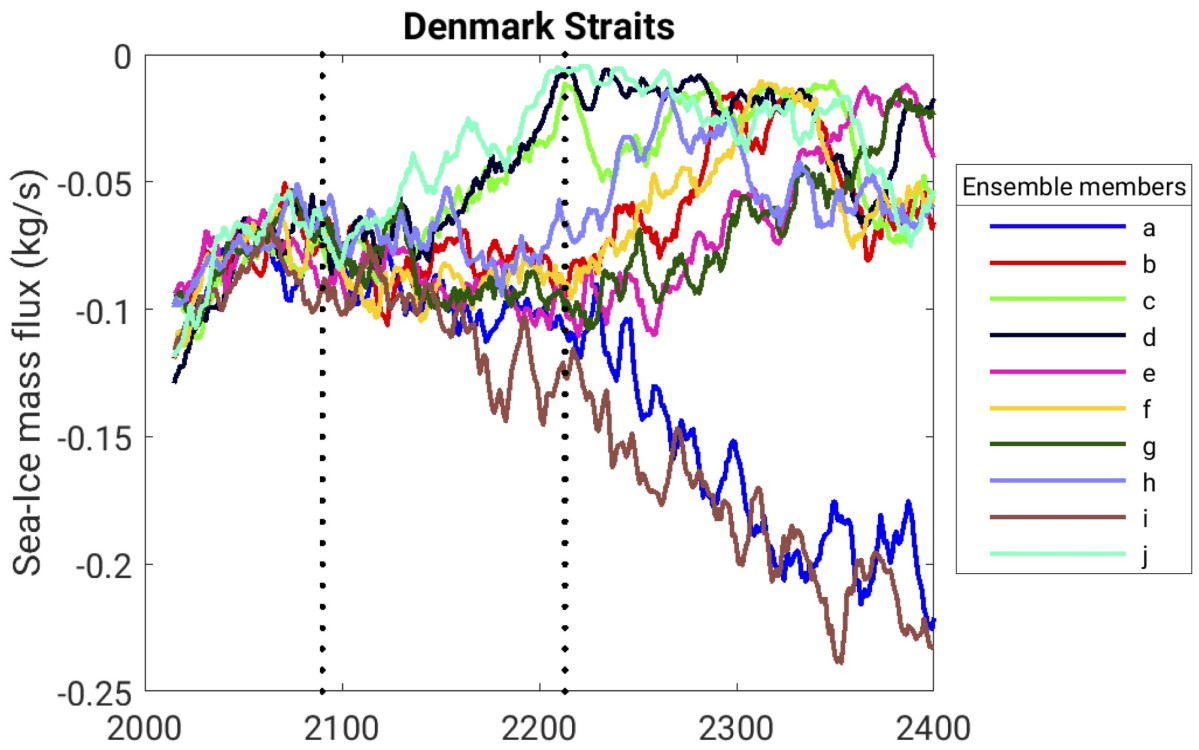


FIG. 5. Annual mean sea ice mass flux (kg/s) across the Denmark Strait in each ensemble member. Vertical dotted lines correspond to times of change in GHG forcing (see Fig. 2a). Timeseries are smoothed with a 10-year running mean filter.

glacial and sea ice melt terms to the rest of the terms in the salinity budget is shown in SMFig. 12. In runs a and i, both of which show continued decline of AMOC throughout the simulation, both ice melt terms continue to increase after 2100 whereas in runs c, d and j (which recover first) these terms decline strongly reaching zero by 2150. In the rest of the ensemble members, the ice melt related terms increase for some time and go to zero successively, as the AMOC recovers in strength. Increased ice melting leads to freshening but also cooling of the surface since the meltwater is at colder temperatures than the surrounding water temperatures. Colder surface, however, will evaporate less producing a positive feedback to the surface freshening.

We therefore conclude that the surface freshening associated with sea ice, which increases drastically, is responsible for initiating the decline of deep convection in IS after 2100 in some of the ensemble members and the near complete shut down in two of them. Sea ice is transported by

the East Greenland Current through the Denmark Strait and into the Irminger Sea where it melts (Fig. 5). A decrease in this transport is associated with recovery of the AMOC. In fact, ensemble members a and i show large, short-term, perturbations in the sea ice mass flux across the Denmark Strait even before 2100 and certainly after the 2150s (Fig. 5).

Enhanced glacial and sea ice melt patterns are centered on the western side of the Irminger Sea and south of the Denmark Strait as sea ice is transported south-westward through the straits by the East Greenland Current. Indeed, ensemble mean sea ice fraction distributions (SMFig.13) show that sea ice extends further south on the western side of the Irminger sea in simulations g and i.

The salinity budgets in the subpolar gyre therefore point to fresh water processes associated with the melting of sea ice, and to a lesser extent land-ice, that stabilize the water column and prohibit deep water formation in the Irminger Sea in some ensemble runs. This process leading to substantial weakening of the AMOC is known to occur in historical observations and has been reproduced in simulations (Holland et al. 2001; Jungclaus et al. 2005; Koenigk et al. 2006).

d. Forced response vs Intrinsic variability

All the ensemble members have the same internal variability that represents the stochasticity of the model's climate, since they are simulations using the same numerical model and the exact same forcing. However, each member is at different phase of the internal variability at different times, with some members being in positive phase and others in negative phase. All model components exhibit internal variability, but in one component the response due to internal variability diverges more among ensemble members. In this section we are investigating which component is driving this response.

To do so, we quantify the relative importance of the stochastic variability in the fresh water inputs vs. the forced signal from the changing GHG forcing, we follow the analysis by Hirschi et al. (2020); Leroux et al. (2018); Grégorio et al. (2015); Holland et al. (2008) who assumed that averaging over the ensemble members eliminates the uncorrelated natural variations so that the ensemble mean describes the forced response, while each member's deviation from the ensemble mean describes the stochasticity, i.e. the internal variability, of the system. This internal (or intrinsic) variability is associated with natural modes of variability in the system, e.g. the El-Nino/Southern Oscillation, the Pacific Decadal Oscillation, the Arctic Oscillation, etc.

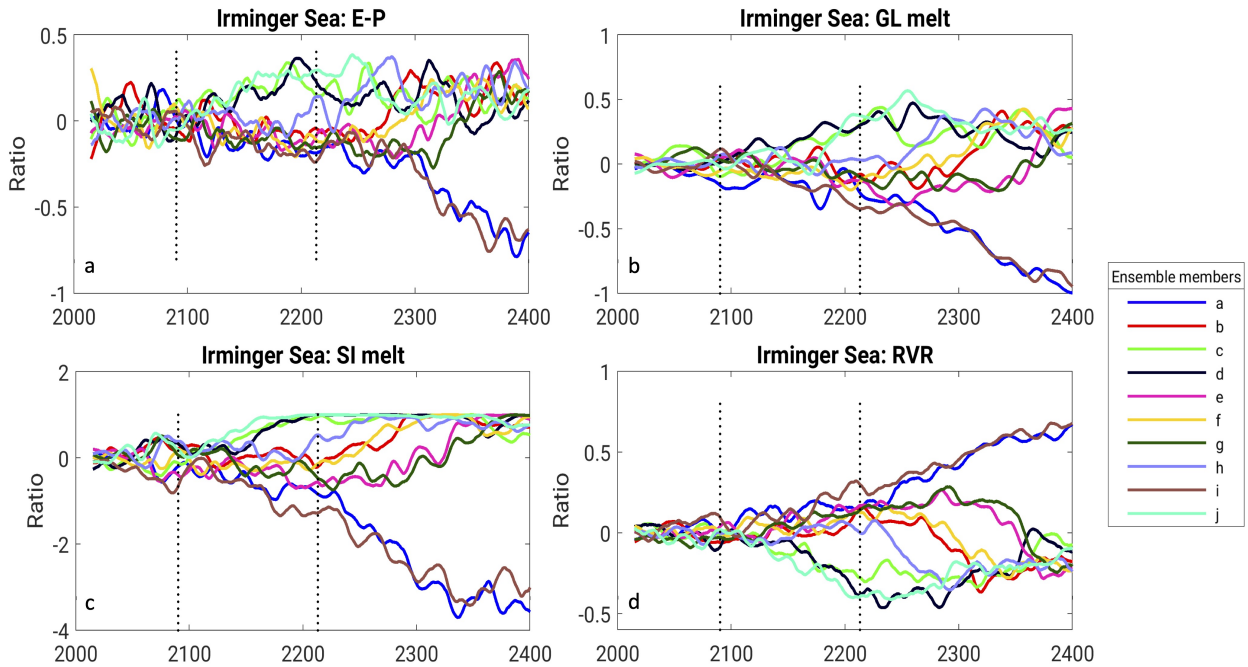


FIG. 6. Ratio of intrinsic-to-forced response for each of the fresh water input terms in the Irminger Sea: (a) E-P, (b) land-ice glacial melt, (c) sea ice melt and (d) rivers. For the ratio, we use the absolute value of the forced response, so that the ratio sign denotes whether the intrinsic variability leads to salinification (positive ratio) or freshening (negative ratio). Timeseries are smoothed with a 10-year running mean filter. Vertical dotted lines correspond to times of change in GHG forcing (see Fig. 2a). Total surface fresh water inputs forced response and intrinsic variability shown in SMFig. 14.

Intrinsic variability in LS fresh water inputs (SMFig. 14) is only about 10% of the forced response and it grows substantially in ensemble members a and i only after 2300. In the IS (SMFig. 14 and Fig. 6a), intrinsic variability in the fresh water inputs amplifies after the early 2100s, with the greatest divergence stemming from the sea ice melt (Fig. 6c).

Therefore, internal variability (or stochasticity) in the modeled climate system plays a critical role in the bifurcation of AMOC, hence this AMOC bistability is an example of noise-induced bifurcation.

e. Role of different feedbacks

In the previous sections we showed that internal variability in ice melt drives the AMOC bifurcation, *initially*. However, while the internal variability is the same in all ensemble members,

the phase of the internal variability that each member has at the time of GHG forcing change may be very different. Different feedbacks may then play an important role in further “pulling apart” the different ensemble members, leading to some having a much stronger AMOC than others. In this section, we provide an overview of different feedbacks that might play a role in enhancing or opposing this bifurcation, following on ideas introduced by Gent (2018); Weijer et al. (2019). A thorough, quantitative analysis of each of these feedbacks, and maybe others that might play a role, as for example was provided in a very interesting study by Swingedouw et al. (2007), is beyond the scope of this paper, but will be the topic of future research.

1) SEA ICE FEEDBACKS

In the ice-evaporation feedback, as land and sea ice melt, the colder meltwater relative to the surrounding water cools the overlying atmosphere, and reduces its water holding capacity, leading to reduced evaporation and even larger surface freshening locally and therefore further reduction in deep water formation. This is a positive feedback to AMOC weakening. SMFig. 12 shows that in ensemble members c,d and j, the E-P term remains more or less constant, while in all other members after 2100 changes in ice-melt are followed by similar changes in E-P.

In the ice-albedo feedback under strong GHG warming, ice melting in land and ocean lowers the albedo locally, which leads to more heat uptake by the ocean and further melting of sea ice, maintaining the AMOC in a weak state. However, if the GHG warming is weak, or starts to decline (as in our case after 2200) the ice-albedo feedback operates differently: if there happens to be more sea ice in the SPG due to internal variability (compare runs g and i for years 2200-2220 in SMFig. 13), this feedback will lead to more sea ice build up, higher albedo and more surface cooling, as we see happen in ensemble member i. The larger sea ice cover insulates the surface ocean from heat losses, and provides more melt water, so that convection cannot start. Albedo change in the Irminger Sea (SMFig. 15) shows clearly abrupt increases in members a and i after 2150, associated with increases in sea ice coverage there (SMFig. 13).

2) LARGE SCALE (OVERTURNING) SALT-ADVECTION FEEDBACK

The strength of the overturning salt-advection feedback is often used as a predictor of AMOC collapse or recovery. It is typically assessed via the fresh water transport by the large-scale overturning circulation (M_{ov}). For example, a positive M_{ov} along 33°S (de Vries and Weber 2005;

Castellana and Dijkstra 2020) or a positive M_{ov} divergence between subArctic North Atlantic along 80°N and Southern Ocean subtropical gyre along 33°S (Li et al. 2021) are proposed as good indicators of whether the AMOC has multiple equilibrium states. A positive M_{ov} indicates that the AMOC transports fresh water into the North Atlantic, so that when the AMOC declines, the fresh water import is reduced, salinity increases and the circulation tends to resume. A positive M_{ov} , represents a negative feedback to AMOC slow down, therefore suggests a mono-stable AMOC regime.

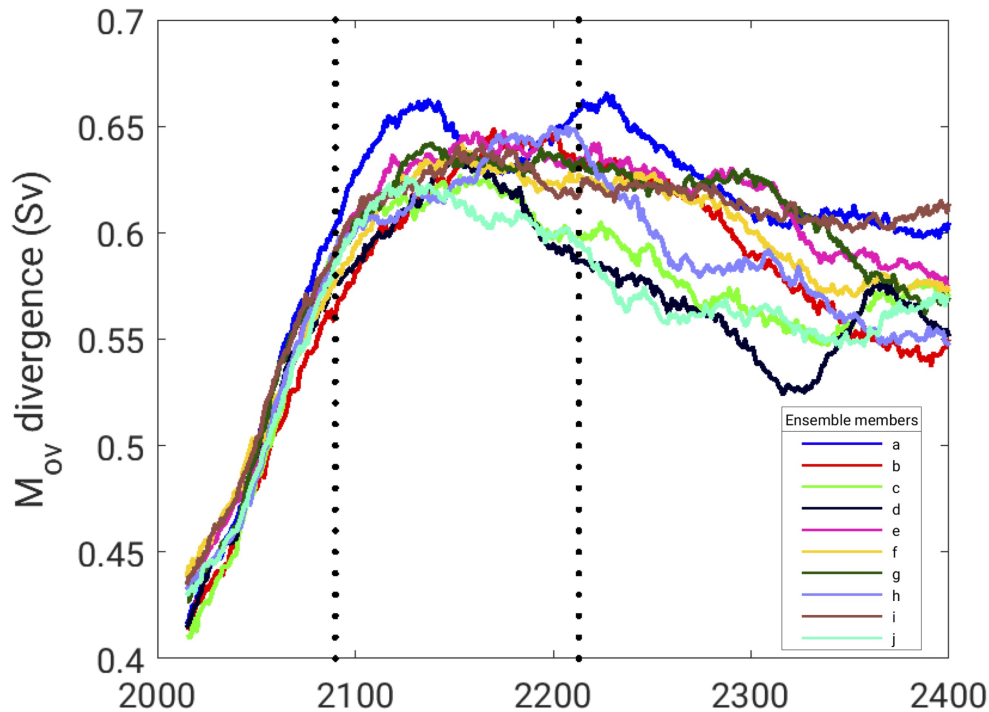


FIG. 7. Divergence of the fresh water transport by the overturning circulation (M_{ov}), between 33°S and 80°N , i.e. $M_{ov}(33^{\circ}\text{S})-M_{ov}(80^{\circ}\text{N})$. Timeseries are smoothed with a 10-year running mean filter. Vertical dotted lines correspond to times of change in GHG forcing (see Fig. 2a).

In the GISS-E2-1-G the M_{ov} divergence between 33°S and 80°N , is positive both in the pre-industrial control simulation (strength =0.3 Sv; figure not shown) and in the SSP2-4.5 scenario (Fig. 7 and SMFig. 16) in all ensemble members. In addition to the divergence, the M_{ov} itself is positive in the South Atlantic between latitudes $35^{\circ}\text{S}-15^{\circ}\text{S}$ (SMFig. 24) in all ensemble members throughout the integration. While, eventually the AMOC in all ensemble members recovers (in members a and i after 800 years of being almost shut down), the salt-advection feedback does

not capture the divergence among ensemble members with regards to stability. Therefore, the large-scale salt-advection feedback alone cannot explain the AMOC bifurcation among ensemble members.

3) LARGE SCALE (OVERTURNING) HEAT-ADVECTION FEEDBACK

The total northward oceanic heat transport declines consistently in all ensemble members (SMFig. 17) from 2015 till 2100. At that point, it remains in a weakened state in run c and further weakens in runs g and i until year 2200(2300) when it starts to recover in run c(g). In run i it gets nearly shut down by 2300.

This slowdown of the northward transport results in additional cooling in the SPG, and is associated with the expansion of the warming hole there (Menary and Wood 2018) which in addition to maintaining sea ice in the SPG, it also directly cools the surface water which acts as a negative feedback to the AMOC decline but at the same time promotes a decrease in evaporation and further freshening, establishing competing negative feedback.

4) ATMOSPHERIC FEEDBACKS

A weakened AMOC leads to widespread cooling in the SPG, i.e. deepening of the warming hole, which leads to further weakening of the AMOC through a complex series of atmosphere-ocean interactions. As shown in Fig. 8, the colder surface air temperatures in run i than in run c (column 1) results in greater sea level pressure in the North Atlantic, primarily over the western portion of the region (column 2). With this sea level pressure configuration, the anticyclonic wind flow results in greater southward velocities to the east of Greenland (column 4), which results in a slight increase in the ocean currents southward in that region (column 6) and is consistent with increased southward (and westward) sea ice flux through the Denmark Strait (columns 7 and 8). Melting of the sea ice then helps sustain the colder temperatures and maintain the reduced AMOC in ensemble i, and its eventual collapse. This is a feedback in the sense that it is dependent upon the SPG cooling associated with the reduced AMOC and diminished oceanic heat transport, and so does not arise originally; but when it does, it helps sustain the sea ice transport through the straits, the colder conditions, and the AMOC collapse (note how strong these feedbacks are by the last period shown, 2361-2380). A similar situation prevails in ensemble run g until 2210, but there is not enough sea ice in this member to maintain the circulation reduction and subsequent effects.

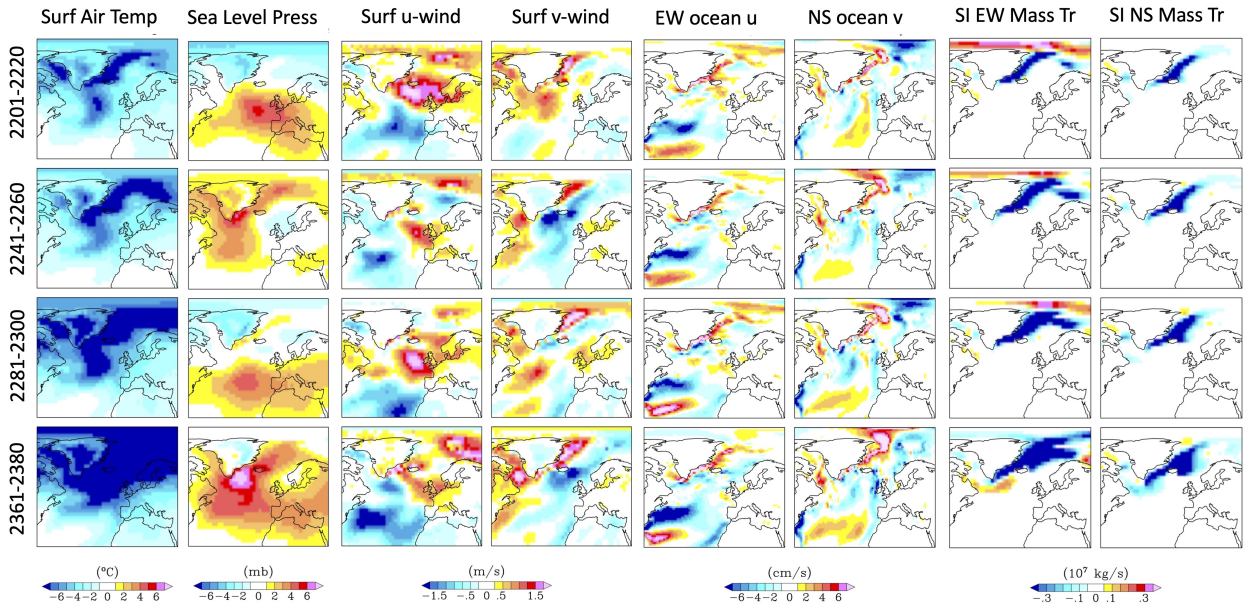


FIG. 8. Difference of atmospheric and oceanic fields between ensemble runs i and c, averaged over DJFM of different 20 year intervals after year 2200. Columns 1) i-c surface air temperature, 2) i-c sea level pressure, 3) i-c surface zonal wind, 4) i-c surface meridional wind, 5) i-c surface zonal ocean current speed, 6) i-c surface meridional ocean current speed, 7) i-c zonal sea ice mass transport, 8) i-c meridional sea ice mass transport.

Another impact of the SPG cooling and the AMOC weakening is a southward/equatorward shift of the maximum heating latitude and of the ITCZ, as well as reduction of precipitation and salinification of the subtropical North Atlantic (Stouffer et al. 2006). These saltier waters are then transported into the SPG triggering convection, deep water formation and AMOC recovery (in all members except a and i).

We focus on the period 2221–2251 which is the time when the GHG forcing starts to decline (Fig. 2a). During this period, AMOC in run c is stable at historical levels (has recovered), AMOC in member g slowly starts to recover while in member i, AMOC continues towards near collapse. Runs g and i have more fresh water inputs (a negative E-P-R compared to run c) over the storm track region and the subpolar North Atlantic (Fig. 9) because as we have seen they are colder and have less evaporation. Over the subtropical North Atlantic, however, excess evaporation in both g and i runs over the c run leads to salinification while the precipitation deficit leads also to salinification: the net effect is large salinification of this region. The effect is larger in the i run than in the g run. Lastly, in the tropical Atlantic we have an excess precipitation that leads

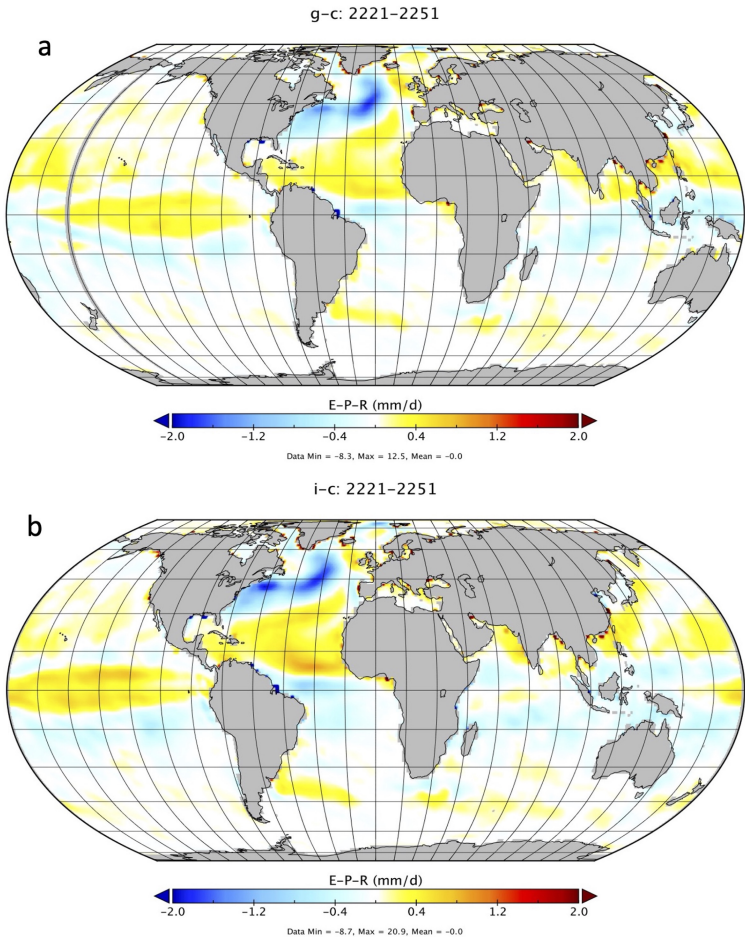


FIG. 9. E-P-R (mm/day) difference in runs g-c (top panel) and i-c (bottom panel) averaged over the period 2221-2251.

to freshening and only a slight excess in evaporation with a net result being reduction of salinity. These atmospheric patterns of surface freshening will further weaken the salt-advection feedback in both g and i members, but more so in run i where the AMOC eventually collapses.

f. Climate consequences

The state of the AMOC has consequences for the North Atlantic but also the global climate (Bellomo et al. 2021). In all ensemble members global mean surface air temperatures rise till 2100 and then either stabilize or decline (as in members a and i, SMFig. 18). The Northern and Southern Hemisphere average temperatures are larger and lower than the global mean temperature respectively, except in members a and i after 2300. After 2300, the Northern Hemisphere becomes

colder than the global mean and the Southern Hemisphere becomes warmer than the global mean. Therefore the collapse of the AMOC at 48°N in ensemble members a and i shifts the location of greatest warming from the Northern Hemisphere to the Southern Hemisphere while reduces the total global warming by a small amount.

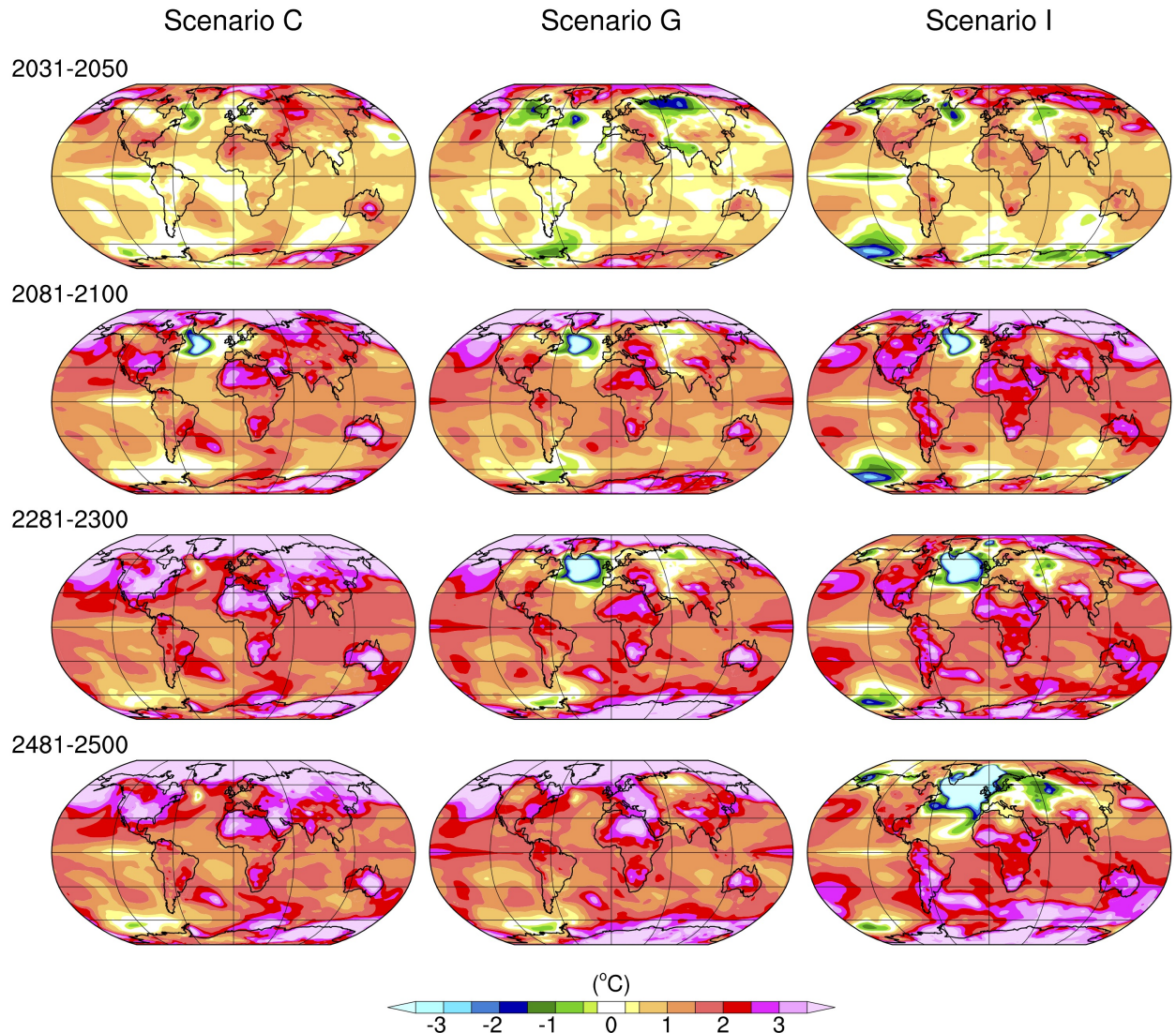


FIG. 10. Surface air temperature change (in deg C) from 2015 in different periods for ensemble members c (left column), g (middle column) and i (right column). Each row represents a 20-yr averaging period denoted on the left most side of the panels.

Temperature anomalies relative to 2015 in ensemble member c (Fig. 10 left column) whose AMOC recovers early, exhibit a high latitude amplification associated with the greenhouse forcing

in SSP2-4.5, primarily in the Northern hemisphere, but with highly significant warming also over the southern and eastern United States, north Africa and eastern Antarctica. The warming stabilizes in the later part of the 23rd Century, following the reduction in the SSP2-4.5 forcing. There is also a relative cooling region (warming hole) developing south of Greenland peaking around 2100, associated with the reduced AMOC during the early period and a corresponding reduction in poleward heat transport from the overturning circulation (SMFig. 17a).

In ensemble member g (Fig 10 middle column) whose AMOC starts to recover later, around 2200, the warming hole is more severe in the late 21st Century, and the high latitude amplification less extensive than in c (see also Table 1, column YR2090 for the Irminger Sea). This relates to the longer duration of the AMOC reduction in g whose full return doesn't occur until around 2400 (at which point it is actually somewhat more active than in c, and so its warming hole is then a little less extensive). Its ocean heat transport has returned to historical values, aided both by the returning overturning circulation as well as the strong gyre transport (SMFig. 17b). Note also that the more extreme warming over the southern and eastern United States, and northern Africa, is not evident in ensemble member g (bottom rows, middle column Fig. 10).

Finally, in ensemble member i (Fig. 10c), the warming hole grows with time until it severely diminishes the high latitude amplification in the Northern hemisphere, resulting in actual cooling over western Europe by 2500, and even eastern Asia, with reduced warming over the east and central United States. Warming over Antarctica and large parts of the Southern Ocean, however, is more extensive (consistent with the amplified Southern Hemisphere warming shown in SMFig. 18). As expected, the ocean heat transport reduction (SMFig. 17c) is more extreme than in other ensemble members, and, along with the overturning circulation, does not recover. Even the gyre circulation produces less poleward heat transport as time goes on. Southern hemisphere warming is consistent with the weakening AMOC that otherwise transports heat northward across the equator (Trenberth and Solomon 1994).

We also examine the alterations in regional precipitation patterns associated with these different ensemble members (Fig. 11). During the period 2031–2050 the differences among the members c, g and i are small and due to internal variability, mostly in the tropics. By 2081–2100, ensemble member c has less precipitation in the North Atlantic and in the tropics than members g and i. However, by 2281–2300, there are now significant precipitation differences: precipitation is

Precipitation Anomalies from Avg Yrs 2015-2035

(20 Yr Avgs)

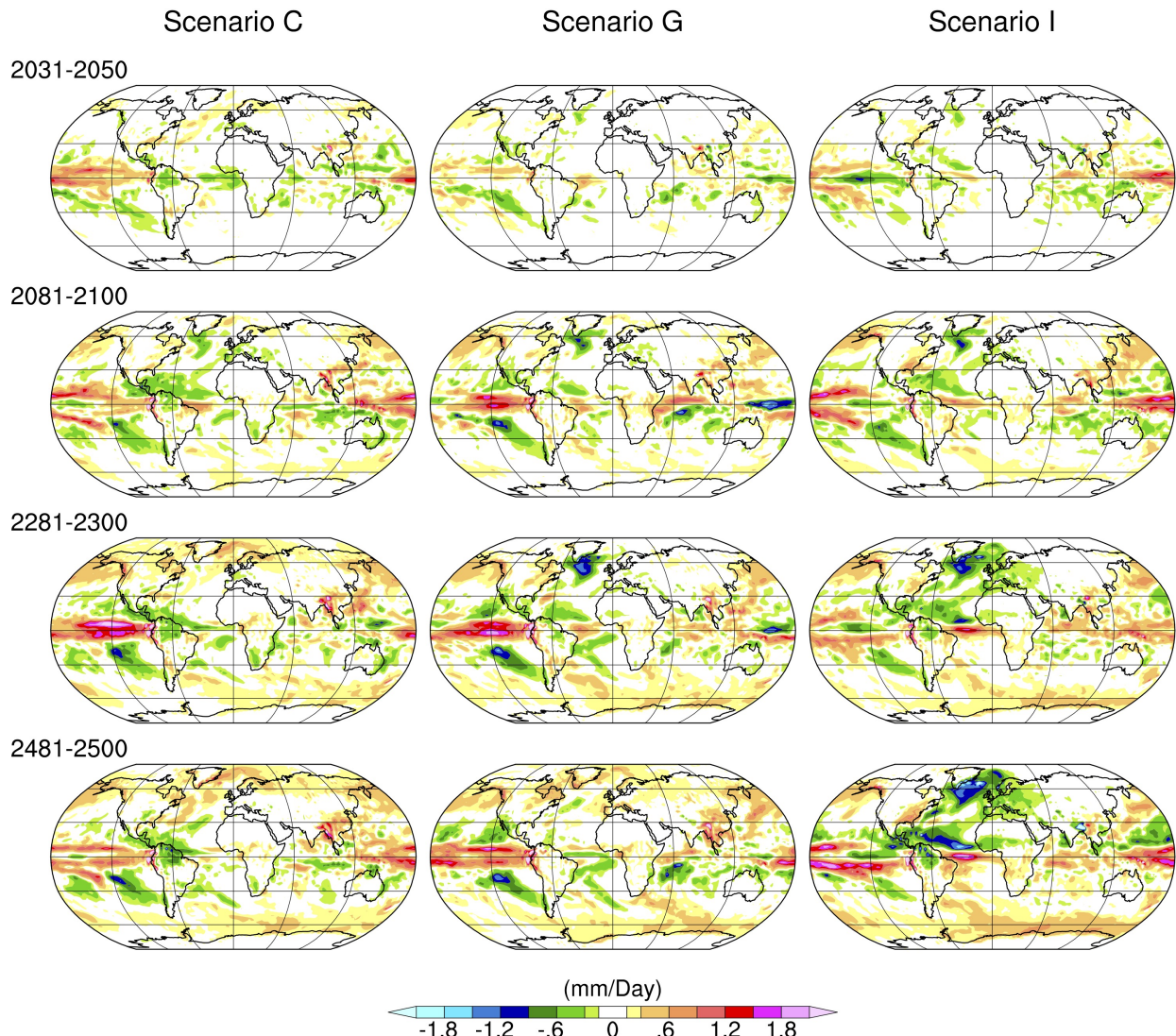


FIG. 11. Precipitation change (mm/day) from 2015 in different periods for ensemble members c (left column), g (middle column) and i (right column). Each row represents a 20-yr averaging period denoted on the left most side of the panels.

reduced throughout the North Atlantic extending into western Europe in run i, and there is less precipitation north of the equator in the Atlantic (see also the section on atmospheric feedbacks). The reduction extends across Africa, and even into the eastern tropical Pacific. By 2481–2500,

AMOC in members c and g has recovered so precipitation differences have largely disappeared, while differences have become more severe in i, associated with the additional reduction in AMOC. Precipitation increases south of the equator, along with reductions to its north, implying a southward shift of the ITCZ.

4. Discussion and Conclusions

We have assessed the AMOC bi-stability in a suite of 10 ensemble member simulations with the GISS-E2-1-G model, all identically forced with the SSP2-4.5 scenario and with slightly different initial conditions in year 1850 in order to sample the model's climate internal variability. After a strong AMOC decline in all the members during the 21st Century, there is a 20% chance for the AMOC in the SPG reaching gradually a near-collapse state (about 1 Sv in year 2400) due to stochastic variability in the land and sea ice melt, reinforced by feedbacks between the atmosphere, the ocean and the ice. Over this time period, the AMOC at 26°N of the near-collapsed ensemble members declines to about 6 Sv. There is a wide spread in AMOC recovery timescales that ranges between 5 and about 800 years.

We found that during the initial phase of strong increase in GHG forcing (years 2015–2090), the ensemble mean AMOC strength decline at 26°N (48°N) was about 9.4 Sv (9.2 Sv) or 40% (52%) of its 2015 value of 23.3 (17.7) Sv. During this period, the AMOC response was highly correlated with deep convection in the Labrador Sea (see section 3b). Subsequently, as the GHG forcing stabilized (2090–2200), the AMOC in three members recovered within 10 years, while in another 5 members, it continued to decline and remained in a weak (unstable) state for periods that ranged from 5 to 200 years, thereafter recovering. The remaining two members reached a stable state with very weak AMOC at 26°N and nearly shutdown at 48°N, which lasted for 800 years, and then they too recovered.

The weak AMOC as well as the nearly AMOC-off states were the result of stochastic freshening of the Irminger Sea through glacial and mainly sea ice melt produced by enhanced transport of ice through the Denmark Strait. Sea ice expansion and retreat triggered other feedbacks such as the ice-evaporation feedback and the ice-albedo feedback, which were found to be highly variable in the areas where the sea ice was thinner (i.e. the margins of the Arctic Ocean and the southern most side of the ice pack). These feedbacks amplified the surface freshening, while horizontal advection

of both salt and heat via the overturning circulation played an important role in the subsequent development of the AMOC. The differences in ensemble members are stochastic, resulting from differences in the phase of the internal variability which are amplified by the local feedbacks.

Our results highlight the role of the SPG convective mixing and deep water formation in the AMOC variability, an effect found in other climate model simulations of current as well as future warming of the world climate (Brodeau and Koenigk 2016; Sgubin et al. 2017; Zou et al. 2019; Gu et al. 2020; Swingedouw et al. 2021). These results are also consistent with observational studies that suggest that Labrador Sea Water variability can trigger large AMOC changes (e.g. Kieke et al. (2006)) as well as more recent measurements from the Overturning in the Subpolar North Atlantic Program (OSNAP) that revealed that the largest fraction of the AMOC variability is mainly driven by the Irminger and Iceland basin mixing rather than the Labrador Sea (Lozier et al. 2019; Menary et al. 2020; Kuznetsova and Bashmachnikov 2021).

The initial response of the AMOC to GHG warming found in the GISS-E2-1-G model is similar to other models. Most CMIP6 climate models show an AMOC transport decline in the 21st Century under SSP2-4.5 by 29% on average, with a fairly wide spread of about 50% (Weijer et al. 2020). The GISS model is among those with the strongest decline, which might be due to the stronger than average AMOC. The GISS-E2-1-G has a too deep subpolar convective mixing that engages a larger area compared to observations, leading to larger volume of NADW, a behavior shared by many other models (Heuzé 2021). The AMOC strength at 26.5°N is 23 ± 1 Sv in the early twenty-first century (Miller et al. 2021), about 30% greater than the RAPID-MOCHA observations suggest for the period post-2004. The simulated GISS North Atlantic Deep Water (NADW) is saltier and denser than observations (Lozier et al. 2019) which also contributes to a stronger AMOC. Moreover, in the GISS-E2-1-G model dense water forming in the GIN Sea does not flow over the sill to join the NADW, a pathway supported by observations (Petit et al. 2020). A possible reason for these biases is the lack of overflow parameterizations for the GIN Sea and the Mediterranean outflows that leads to biases in the subpolar and subtropical North Atlantic hydrography and geostrophic currents. GISS-E2-1-G also has greater sea ice area in the Northern hemisphere than observations suggest by about 30% for the historical era (Miller et al. 2021) which Kelley et al. (2020) attributed to excessive radiative loss at high latitudes related to brighter clouds. Lastly, several studies (Manabe and Stouffer 1994; Thomas and Fedorov 2019)

claim that subsurface density increases during hosing experiments may contribute to the AMOC recovery, but such an effect is not found in our simulations (see SMFigs 21,22,23). These maybe important caveats/discrepancies from other modeling studies of the results shown here.

Sea ice related intrinsic variability was found here to play a critical role in disrupting convection in the Irminger Sea and therefore affecting the AMOC strength. Subpolar North Atlantic freshening due to transport from higher latitudes that takes the form of sporadic pulse-like events is long understood not only to affect local climate and weather patterns but the AMOC variability as well (Chafik and Holliday 2022). Castellana and Dijkstra (2020) suggested that noise-induced changes might lead to the possibility of both present-day and collapsed AMOC states within the CMIP5 models, when abrupt cold and freshening events led to sea ice advance (Klus et al. 2018). Sea ice intrinsic variability can lead to threshold instabilities in the SPG (Holland et al. 2008) while extreme events of fresh water transport can cause tipping points in deep water formation and even AMOC collapse (Sgubin et al. 2017). The GISS-E2-1-G model's large intrinsic variability has been documented in Kelley et al. (2020) and is, together with the changing GHG forcing, apparently the underlying cause of the AMOC bifurcation in our simulations. In the SSP2-4.5 we found a large part of the variance and inter-ensemble spread of AMOC to be associated with sea ice melt. Ice-melt feedbacks by E-P and albedo could enhance the effects of the stochastic variability in fresh water inputs at the surface of the ocean and would oppose the overturning salt-advection feedback locally.

A widely used predictor of the AMOC stability (Rahmstorf 1996; de Vries and Weber 2005; Weber et al. 2007) that relates AMOC equilibrium states to the large-scale fresh water transport across a latitude in the South Atlantic subtropical gyre via the overturning circulation, failed to explain the bistability of the AMOC in our model. Mecking et al. (2017) suggested that models with too strong AMOC (like ours) have positive M_{ov} in the Southern Ocean subtropical gyre and thus should exhibit a monostable AMOC. In our model all ensemble members AMOC eventually recovered within 800 years, indicating that over very long timescales (more than 800 years) the AMOC is monostable. However, in timescales shorter than this, the salt-advection feedback is not enough to explain the AMOC bifurcation. Even in the CMIP5 generation GISS model (GISS-E2-0-R) (Rind et al. 2018), it was shown that poleward of 40°N in the North Atlantic, salt transport did not change with the cessation of the overturning circulation. That study as well as the current

one show that atmospheric transports and feedbacks (which are usually muted when there is an externally prescribed fresh water flux) cannot be neglected, as the continued enhanced atmospheric transport of latent heat for fresh water forcing in the warming climate, even during the AMOC shutdown, was an important factor in maintaining the shutdown. These studies also show that there is an important caveat in using ocean-only models in hosing experiments: these models have some potentially strong restoring at the surface, mainly in the sea surface salinity fields, which can counteract the fresh water forcing.

The importance of AMOC bistability has been demonstrated in several paleoclimate studies which linked large swings in AMOC strength due to abrupt climate change. The 8.2 kyr event was coincident with cataclysmic drainage of the glacial Lakes Agassiz and Ojibway into the Hudson Bay which probably led to a significant decline of North Atlantic Deep Water production that cooled the Northern hemisphere but not the entire globe (LeGrande et al. 2006). During the Younger Dryas 12000 years ago, a large export of fresh water from Lake Agassiz through the St Lawrence drainage (Rooth 1982) is hypothesized to have led to a temporary shutdown of the AMOC (Broecker 2000). It ended quite rapidly, with strong temperature increases in Greenland, of the order of 10°C in 100 years (Kobashi et al. 2008). As shown in SMFig. 18, ensemble members e and g had temperature increases of 4–5°C in the time period between 2300 and 2400 (specifically at the Greenland Ice Sheet Project Two (GISP2) location in Greenland), and rapid temperature rises are a feature of all the runs with returning AMOCs. A more complete discussion of the potential relationship between the Younger Dryas and AMOC collapse during future warming can be found in the supplementary data of Rind et al. (2018), a study that described AMOC collapse and recovery in some configurations of the CMIP5 GISS-E2-R model. Also of relevance are Heinrich events, a series of at least six large discharges of icebergs that occurred between approximately 60,000 and 16,800 years ago and carried coarse-grained rocky debris, apparently from North American ice sheets, into the North Atlantic Ocean at latitudes between 40 and 55°N during the last glacial period (Zhang et al. 2017). Heinrich events are thought to be associated with significant AMOC reductions which may have led to cooling of the North Atlantic (Menviel et al. 2014) or triggered subsurface ocean warming that led to ice-shelves collapse (Bassis et al. 2017). These events occurred abruptly in roughly 8,000–9,000 year cycles and lasted between about 200 and 2,300 years. Dansgaard-Oeschger events, more frequent than Heinrich events with

25 occurrences between about 80,000 and 8,000 years ago, also featured millennial-scale climate shifts in air temperatures over Greenland between extremely cold stadial conditions and relatively mild interstadial periods. They may have been triggered by large amounts of fresh water from melting ice sheets during the warmer periods (e.g., Clark (2001)).

The key point here is that the CMIP6 GISS model is very close to an AMOC-threshold which has allowed us to investigate how stochastic variability can push the system into an AMOC-on or a nearly AMOC-off state that last for several centuries. While in the 8.2 kyr, Younger Dryas or Heinrich events, the circulation change was forced (perhaps) by fresh water inputs and was not likely the result of stochastic forcing nudging the system over a threshold, the D-O events are more suggestive of spontaneous collapses. In any case, our model behavior suggests that we could look for stochastic variations as precursors to prior analogs in the paleoclimate record.

Regimes in which multiple equilibria are possible may be a very important characteristic of the global ocean circulation and the climate system, in many different geological eras. As Jackson and Wood (2018) point out, a key question is whether the AMOC will remain stable in the future or transition to a weak state or even collapse, and if it does collapse, whether it will recover and how long that might take (Rind et al. 2018). It is therefore important to know how close we are to an AMOC tipping point or threshold, whether a shutdown AMOC state is possible, and if so, under what conditions might it recover, and whether current climate intrinsic variability alone can push the AMOC over that threshold. Our simulations suggest there is a “sweet-spot” between sea ice growth and GHG warming that may lead to an unstable and nearly collapsed AMOC, but whether this is reflective of the real world is currently unknown. Our results highlight the need for additional multi-century simulations and coordinated model intercomparisons under extended (beyond 21st and 22nd Centuries) and varying low warming forcings which may couple with intrinsic variability and lead to tipping points.

Acknowledgments. The authors wish to thank 3 anonymous reviewers for their input which greatly improved the manuscript. Funding was provided by the NASA-Modeling, Analysis Modeling and Prediction program (MAP) (grant number NNX16AC93 G, under Principal Investigator Anastasia Romanou). Climate modeling at GISS is supported by the NASA Modeling, Analysis and Prediction program, and resources supporting this work were provided by the NASA High-End

Computing (HEC) Program through the NASA Center for Climate Simulation (NCCS) at Goddard Space Flight Center.

Data availability statement. All CMIP6 data used in this study is available from the Earth System Grid Federation (ESGF) <https://esgf-node.llnl.gov/search/cmip6/> or from the NASA Center for Climate Simulations (NCCS) https://portal.nccs.nasa.gov/dashshare/giss_cmip6/. The specific simulations used here are the historical r[1-10]i1p1f2 (doi: 10.22033/ESGF/CMIP6.7127) and ssp245 r[1-10]i1p1f2 (doi: 10.22033/ESGF/CMIP6.7415). All GISS ModelE components are open source and available at <https://www.giss.nasa.gov/tools/modelE/>.

APPENDIX

Salinity Budget calculations

The salinity budget equation (Eq. 1) expresses the change of the vertically integrated salinity due to processes such as horizontal advection upwelling/downwelling (i.e. vertical advection at 1000 m), vertical mixing (at 1000 m) and surface fresh water inputs. Additionally, in the subpolar regions, near convection sites, the fresh water inputs from rivers, sea ice and land ice (glacial melt) are not negligible and have to be explicitly accounted for in the budget:

$$\frac{\partial s}{\partial t} = -\nabla \cdot (s\mathbf{u}) + \frac{\partial}{\partial z} \left(K_v \frac{\partial s}{\partial z} \right) + \sum_i F_i \delta(z - \eta) \quad (\text{A1})$$

where s is the salinity in psu, \mathbf{u} is the ocean velocity vector in ms^{-1} , following the convention that direction of u is eastward, v is northward, and w is upward, K_v is the vertical diffusivity in m^2s^{-1} and $\sum F_i$ is the sum of fresh water fluxes through the ocean surface due to different processes in $\text{kg},\text{salt}/\text{kg},\text{water}/\text{s}$. The index i corresponds to evaporation minus precipitation (E-P), sea ice melt, sea ice formation, land-ice (glacial) melt, and riverine outflow i.e.

$$\sum_i F_i = F_{E-P} + F_{ICEm} + F_{ICEf} + F_{RVR} + F_{ICEgl} \quad (\text{A2})$$

where $\delta(z - \eta)$ is the Dirac function, equal to 1 at the free surface (η) and zero elsewhere. We note here that we have extended the integration to different depths below 1000m, but the results are

virtually unchanged because the deeper layers contribute very little to the salinity budget relative to the upper layers.

Integrating Eq. (1) first vertically and then spatially over each region shown in Fig. 1b, i.e. the Labrador Sea and the Irminger Sea, using the divergence theorem, we get:

$$\int_A \int_H^\eta \frac{\partial s}{\partial t} dz da = \int_H^\eta \left(\int_S vs dx - \int_N vs dx + \int_W us dy - \int_E us dy \right) dz \quad (\text{A3})$$

$$+ \iint [(ws)|_H - (ws)|_\eta] dx dy + \iint [(K_v \frac{\partial s}{\partial z})|_H - (K_v \frac{\partial s}{\partial z})|_\eta] dx dy \\ + \Sigma_i \iint F_i dx dy \quad (\text{A4})$$

where the N, S, E and W denote the integration along the north, south, east and west boundary respectively. Each of the transport terms is the sum of the large scale and the eddy components. Assuming that vertical advection and diffusion at the surface η are zero, we get:

$$\frac{\partial}{\partial t} \langle \bar{s} \rangle = \langle \bar{vs} \rangle |_S - \langle \bar{vs} \rangle |_N + \langle \bar{us} \rangle |_W - \langle \bar{us} \rangle |_E + \langle (ws)|_H \rangle + \langle (K_v \frac{\partial s}{\partial z})|_H \rangle + \Sigma_i \langle F_i \rangle \quad (\text{A5})$$

where brackets and overbars denote area and depth integration respectively. The left side in Eq. (5) represents the salinity change over the region while the first four terms on the right hand-side represent the convergence of the horizontal transport in the north-south direction and in the east-west direction. The fifth and sixth terms are the area integrated salinity entrainment and diffusion respectively, both evaluated at 1000 m depth. The last term is the sum of all the area integrated surface fresh water inputs, via E-P changes, riverine inputs, sea ice and glacial ice melt and sea ice formation. All terms are expressed in psu/yr. Details on the exact salinity budget derivation in the GISS-E2-1-G model are provided in the Appendix.

Salinity Budget calculation in terms of overturning, gyre and eddy components

The salinity budget transport decomposition in terms of zonal and azonal components (Lobelle et al. (2022)) is:

$$f = f_{zonal} + f_{az}$$

where f is velocity or salinity. The azonal term is associated with the gyre circulation. Note here that both the zonal and the azonal part of the velocity field include the resolved velocities as well as the mesoscale eddy velocities.

The transport across each boundary in Eq. (4) can then be rewritten as:

$$\begin{aligned} \iint v S dx dz &= \iint (v_{zonal} + v_{az})(s_{zonal} + s_{az}) dx dz \\ &= \iint (v_{zonal} s_{zonal} + v_{az} s_{az}) dx dz \end{aligned} \quad (\text{A6})$$

where the cross products of the higher order terms are zero. The zonal term can be further decomposed into a vertically-zonally averaged component f_{net} and a zonally integrated component that varies with depth, the latter associated with the overturning circulation:

$$f_{zonal} = f_{net} + f_{ov}$$

where again f is velocity or salinity.

The transport terms in Eq. (5) take the form:

$$\langle \bar{v} \bar{s} \rangle |_N = \iint v s dx dz = H L_x (v_{net} s_{net}) + L_x \int (v_{ov} s_{ov}) dz + \iint (v_{az} s_{az}) dx dz \quad (\text{A7})$$

where L_x and H are the zonal extent of the section and the vertical extent of the domain. All advection terms in Eq. (5) can be decomposed as in Eq. (7) to highlight the contributions from the large scale overturning circulation and the basin scale gyre circulation. The gyre, overturning and eddy components of the fresh water flux and the salt and heat fluxes are expressed in units of Sv, Sv, and W, respectively.

Conversion of mass budget terms into salinity tendency terms in GISS-E2-1-G

The ocean component in GISS-E2-1-G carries salt (S in kg,salt) and total water mass (M in kg,water) independently. Since salt and fresh water fluxes both contribute to the tendency of salinity averaged over a given mass of the ocean, we combine the budgets of salt S and total seawater M into salinity tendencies ds/dt using the quotient rule:

$$\frac{\partial S}{\partial t} = -\nabla \cdot (S\mathbf{u}) + \frac{\partial}{\partial z}(K_v \frac{\partial S}{\partial z}) + F_{ICEf} \quad (\text{A8})$$

where S is the salt mass in kg,salt, and F_{ICEf} is the salt flux added to the ocean during ice formation.

The ocean mass equation is

$$\frac{\partial M}{\partial t} = -\nabla \cdot (M\mathbf{u}) + \frac{\partial}{\partial z}(K_v \frac{\partial M}{\partial z}) + F_{E-P} + F_{ICEm} + F_{ICEgl} + F_{RVR} \quad (\text{A9})$$

where M is the ocean mass (=fresh water + salt) in kg,water, and F are the fresh water inputs at the surface through evaporation minus precipitation, sea ice melt, glacial ice melt, and rivers, all given in kg,water/s.

Vertically and area averaging both Eq. (A8) and (A9) we get

$$\frac{\partial}{\partial t}\langle\bar{S}\rangle = \langle\bar{vS}\rangle|_S - \langle\bar{vS}\rangle|_N + \langle\bar{uS}\rangle|_W - \langle\bar{uS}\rangle|_E + \langle(wS)|_H\rangle + \langle(K_v \frac{\partial S}{\partial z})|_H\rangle + \langle F_{ICEf} \rangle \quad (\text{A10})$$

$$\frac{\partial}{\partial t}\langle\bar{M}\rangle = \langle\bar{vM}\rangle|_S - \langle\bar{vM}\rangle|_N + \langle\bar{uM}\rangle|_W - \langle\bar{uM}\rangle|_E + \langle(wM)|_H\rangle + \langle(K_v \frac{\partial M}{\partial z})|_H\rangle + \sum_i \langle F_i \rangle \quad (\text{A11})$$

Using the quotient rule, the equation for salinity, s in kg,salt/kg,water=1000*psu, is calculated as:

$$\frac{\partial\langle\bar{s}\rangle}{\partial t} = \frac{\partial}{\partial t}\left(\frac{\langle\bar{S}\rangle}{\langle\bar{M}\rangle}\right) = \frac{1}{\langle\bar{M}\rangle}\frac{\partial\langle\bar{S}\rangle}{\partial t} - \frac{\langle\bar{S}\rangle}{\langle\bar{M}\rangle^2}\frac{\partial\langle\bar{M}\rangle}{\partial t} \quad (\text{A12})$$

The total horizontal advection terms for salinity are therefore:

$$\frac{1}{\langle\bar{M}\rangle}\left(\langle\bar{vS}\rangle|_S - \langle\bar{vS}\rangle|_N + \langle\bar{uS}\rangle|_W - \langle\bar{uS}\rangle|_E\right) - \frac{\langle\bar{S}\rangle}{\langle\bar{M}\rangle^2}\left(\langle\bar{vM}\rangle|_S - \langle\bar{vM}\rangle|_N + \langle\bar{uM}\rangle|_W - \langle\bar{uM}\rangle|_E\right) \quad (\text{A13})$$

The total entrainment at H=1000 m depth is:

$$\frac{1}{\langle M \rangle} \langle (wS)|_H \rangle - \frac{\langle \bar{S} \rangle}{\langle M \rangle^2} \langle (wM)|_H \rangle \quad (\text{A14})$$

The total diffusion at H=1000 m depth is:

$$\frac{1}{\langle M \rangle} \langle (K_v \frac{\partial S}{\partial z})|_H \rangle - \frac{\langle \bar{S} \rangle}{\langle M \rangle^2} \langle (K_v \frac{\partial M}{\partial z})|_H \rangle \quad (\text{A15})$$

while the total surface fresh water inputs are:

$$\frac{1}{\langle M \rangle} \langle F_{ICEf} \rangle - \frac{\langle \bar{S} \rangle}{\langle M \rangle^2} \sum_i \langle F_i \rangle \quad (\text{A16})$$

All terms in A1-9 are given in psu/yr.

The surface fresh water inputs are evaporation, precipitation, ice formation, ice melt, river discharge, and iceberg input. Salt is present in vertical fluxes associated with sea ice formation and sea ice melt. The bottom flux of M is the advective vertical mass flux, and includes both resolved and mesoscale-induced components. The bottom flux of S includes this vertical advection and the vertical flux from the small-scale vertical mixing scheme. The small-scale mixing scheme does not vertically transport total seawater mass. The side fluxes of M and S include both resolved and mesoscale transports within the ocean model, as well as sea ice advection.

References

- Bassis, J. N., S. V. Petersen, and L. Mac Cathles, 2017: Heinrich events triggered by ocean forcing and modulated by isostatic adjustment. *Nature*, **542** (7641), 332–334, <https://doi.org/10.1038/nature21069>.
- Bellomo, K., M. Angeloni, S. Corti, and J. vonHardenberg, 2021: Future climate change shaped by inter-model differences in atlantic meridional overturning circulation response. *Nature Comm.*, **12** (1), 1–10.
- Bitz, C., and W. Lipscomb, 1999: An energy-conserving thermodynamic model of sea ice. *J. Geophys. Res.*, **104**, 15 669–15 677.

- Blunier, T., and E. Brook, 2001: Timing of millennial-scale climate change in antarctica and greenland during the last glacial period. *Science*, **291** (Jan.), 109–112.
- Brodeau, L., and T. Koenigk, 2016: Extinction of the northern oceanic deep convection in an ensemble of climate model simulations of the 20th and 21st centuries. *Clim. Dyn.*, **46** (9-10), 2863–2882, <https://doi.org/10.1007/s00382-015-2736-5>.
- Broecker, W. S., 2000: Abrupt climate change: Causal constraints provided by the paleoclimate record. *Earth-Sci. Rev.*, **51**, 137? 154.
- Bryan, F. O., 1986: High-latitude salinity effects and interhemispheric thermohaline circulations. *Nature*, **323**, 301?304.
- Bryden, H., 2011: South atlantic overturning circulation at 24s. *J. Mar. Res.*, **69**, 38?55.
- Buckley, M. W., and J. Marshall, 2016: Observations, inferences, and mechanisms of the Atlantic Meridional Overturning Circulation: A review. *Rev. Geophys.*, **54** (1), 5–63, <https://doi.org/10.1002/2015RG000493>.
- Caesar, L., S. Rahmstorf, and G. Feulner, 2021: Reply to Comment on 'On the relationship between Atlantic meridional overturning circulation slowdown and global surface warming'. *Env. Res. Lett.*, **16** (3), <https://doi.org/10.1088/1748-9326/abc776>.
- Castellana, D., and H. A. Dijkstra, 2020: Noise-induced transitions of the Atlantic Meridional Overturning Circulation in CMIP5 models. *Scientific Reports*, **10** (1), 1–9, <https://doi.org/10.1038/s41598-020-76930-5>, URL <https://doi.org/10.1038/s41598-020-76930-5>.
- Chafik, L., and N. P. Holliday, 2022: Rapid communication of upper-ocean salinity anomaly to deep waters of the iceland basin indicates an amoc short-cut. *Geophys. Res. Lett.*, **49**, <https://doi.org/10.1029/2021GL097570>.
- Clark, P. U. e. a., 2001: Freshwater forcing of abrupt climate change during the last glaciation. *Science*, **293**, 283–287, <https://doi.org/10.1126/science:1062517>.
- Dansgaard, W., S. J. Johnsen, H. B. Clausen, D. Dahl-Jensen, N. S. Gundestrup, and C. U. e. a. Hammer, 1993: Evidence for general instability of past climate from a 250?kyr ice?core record. *Nature*, **364** (6434).

- de Abreu, L., N. Shackleton, J. Schoenfeld, M. Hall, and M. Chapman, 2003: Millennial-scale oceanic climate variability off the western iberian margin during the last two glacial periods. *Mar. Geol.*, **196** (1), 1?20, [https://doi.org/10.1016/S0025-3227\(03\)00046-X](https://doi.org/10.1016/S0025-3227(03)00046-X).
- de Vries, P., and S. L. Weber, 2005: The Atlantic freshwater budget as a diagnostic for the existence of a stable shut down of the meridional overturning circulation. *Geophys. Res. Lett.*, **32** (9), 1–4, <https://doi.org/10.1029/2004GL021450>.
- Drijfhout, S. S., S. L. Weber, and E. van der Swaluw, 2011: The stability of the MOC as diagnosed from model projections for pre-industrial, present and future climates. *Clim. Dyn.*, **37** (7-8), 1575–1586, <https://doi.org/10.1007/s00382-010-0930-z>.
- Eyring, V., S. Bony, G. A. Meehl, C. A. Senior, B. Stevens, R. J. Stouffer, and K. E. Taylor, 2016: Overview of the Coupled Model Intercomparison Project Phase 6 (CMIP6) experimental design and organization. *Geosci. Mod. Dev.*, **9** (5), 1937–1958, <https://doi.org/10.5194/gmd-9-1937-2016>.
- Garzoli, S., B. MO, D. S, P. RC, and Y. Q, 2013: South atlantic meridional fluxes. *Deep Sea Res. I*, **71**.
- Gent, P. R., 2018: A commentary on the atlantic meridional overturning circulation stability in climate models. *Ocean Model.*, **122**, 57–66, <https://doi.org/10.1016/j.ocemod.2017.12.006>.
- Gent, P. R., J. Willebrand, T. J. McDougall, and J. C. McWilliams, 1995: Parameterizing eddy-induced tracer transports in ocean circulation models. *J. Phys. Oceanogr.*, **25**, 463–474.
- Grégoorio, S., T. Penduff, G. Sérazin, J. M. Molines, B. Barnier, and J. Hirschi, 2015: Intrinsic variability of the atlantic meridional overturning circulation at interannual-to-multidecadal time scales. *J. Phys. Oceanogr.*, **45** (7), 1929–1946, <https://doi.org/10.1175/JPO-D-14-0163.1>.
- Gu, S., Z. Liu, and L. Wu, 2020: Time Scale Dependence of the Meridional Coherence of the Atlantic Meridional Overturning Circulation. *J. Geophys. Res.: Oceans*, **125** (3), 1–10, <https://doi.org/10.1029/2019JC015838>.
- Hawkins, E., R. S. Smith, L. Allison, J. Gregory, T. Woollings, H. Pohlmann, and B. de Cuevas, 2011: Bistability of the atlantic overturning circulation in a global climate model and links

to ocean freshwater transport. *Geophys. Res. Lett.*, **38** (L10605), <https://doi.org/10.1029/2011GL047208>.

Heuzé, C., 2021: Antarctic Bottom Water and North Atlantic Deep Water in CMIP6 models. *Ocean Science*, **17** (1), 59–90, <https://doi.org/10.5194/os-17-59-2021>.

Hirschi, J. J., and Coauthors, 2020: The Atlantic Meridional Overturning Circulation in High-Resolution Models. *J. Geophys. Res.: Oceans*, **125** (4), 1–35, <https://doi.org/10.1029/2019JC015522>.

Holland, M., C. Bitz, M. Eby, and A. Weaver, 2001: The role of iceo-cean interactions in the variability of the north atlantic thermohaline circulation. *J. Clim.*, **14**, 656?675, [https://doi.org/10.1175/1520-0442\(2001\)014<0656:TROIOI>2.0.CO;2](https://doi.org/10.1175/1520-0442(2001)014<0656:TROIOI>2.0.CO;2).

Holland, M. M., C. M. Bitz, L. B. Tremblay, and D. A. Bailey, 2008: The role of natural versus forced change in future rapid summer arctic ice loss. *Geophys. Monograph Series*, **180**, 133–150, <https://doi.org/10.1029/180GM10>.

Hu, A., and Coauthors, 2012: Role of the bering strait on the hysteresis of the ocean conveyor belt circulation and glacial climate stability. *Proc. Nat. Acad. Sci.*, **109** (17), 6417?6422, <https://doi.org/10.1073/pnas.1116014109>.

Huisman, S., M. den Toom, H. Dijkstra, and S. Drijfhout, 2010: An indicator of the multiple equilibria regime of the atlantic meridional overturning circulation. *J. Phys. Oceanogr.*, **40**, 551?567.

Jackson, L. C., and R. A. Wood, 2018: Hysteresis and Resilience of the AMOC in an Eddy-Permitting GCM. *Geophys. Res. Lett.*, **45** (16), 8547–8556, <https://doi.org/10.1029/2018GL078104>.

Jansen, M. F., L.-P. Nadeau, and T. M. Merlis, 2018: Transient versus equilibrium response of the ocean’s overturning circulation to warming. *J. Clim.*, **31** (13), 5147?5163, <https://doi.org/10.1175/JCLI-D-17-0797>.

Jungclaus, J., H. Haak, M. Latif, and U. Mikolajewicz, 2005: Arctic-north atlantic interactions and multidecadal variability of the meridional over- turning circulation. *J. Clim.*, **18**, 4013?4031, <https://doi.org/10.1175/JCLI3462.1>.

Kelley, M., and Coauthors, 2020: GISS-E2.1: Configurations and Climatology. *J. Adv. Mod. Earth Syst.*, **12** (8), <https://doi.org/10.1029/2019MS002025>.

Kieke, D., M. Rhein, L. Stramma, W. Smethie, D. LeBel, and W. Zenk, 2006: Changes in the cfc inventories and formation rates of upper labrador sea water, 1997?2001. *J. Phys. Oceanogr.*, **36**, [@.](https://doi.org/doi.org/10.1175/JPO2814.1.)

Kilbourne, K. H., and Coauthors, 2022: Atlantic circulation change still uncertain. *Nature Geoscience*, **15** (3), 165–167, <https://doi.org/10.1038/s41561-022-00896-4>.

Klus, A., M. Prange, V. Varma, L. Bruno Tremblay, and M. Schulz, 2018: Abrupt cold events in the North Atlantic Ocean in a transient Holocene simulation. *Climate of the Past*, **14** (8), 1165–1178, <https://doi.org/10.5194/cp-14-1165-2018>.

Kobashi, T., J. Severinghaus, and M. Barnola, 2008: $4\pm1^{\circ}\text{C}$ abrupt warming 11,270 yr ago identified from trapped air in greenland ice. *Earth and Plan. Scie. Lett.*, **268** (3-4), 397–407, <https://doi.org/doi.org/10.1016/j.epsl.2008.01.032>.

Koenigk, T., U. Mikolajewicz, H. Haak, and J. Jungclaus, 2006: Variability of fram strait sea ice export: causes, impacts and feedbacks in a coupled climate model. *Clim Dyn*, **26**, 17?34, <https://doi.org/10.1007/s00382-005-0060-1>.

Kuznetsova, D. A., and I. L. Bashmachnikov, 2021: On the Mechanisms of Variability of the Atlantic Meridional Overturning Circulation (AMOC). *Oceanology*, **61** (6), 803–814, <https://doi.org/10.1134/s0001437021060072>.

Large, W. G., J. C. McWilliams, and S. C. Doney, 1994: Oceanic vertical mixing: A review and a model with non-local boundary layer parameterization. *Rev. Geophys.*, **32**, 363–403.

LeGrande, A. H., G. A. Schmidt, D. T. Shindell, C. V. Field, R. L. Miller, D. M. Koch, G. Faluvegi, and G. Hoffmann, 2006: Consistent simulations of multiple proxy responses to an abrupt climate change event. *Proceedings of the National Academy of Sciences of the United States of America*, **103** (4), 837–842, <https://doi.org/10.1073/pnas.0510095103>.

Lenton, T., H. H. K. E. H. JW, L. W, and R. S. et al, 2008: Tipping elements in the earth's climate system. *PNAS*, **105**, 1786?1793.

Leroux, S., T. Penduff, L. Bessières, J. M. Molines, J. M. Brankart, G. Sérazin, B. Barnier, and L. Terray, 2018: Intrinsic and atmospherically forced variability of the AMOC: Insights from a large-ensemble ocean hindcast. *J. Clim.*, **31** (3), 1183–1203, <https://doi.org/10.1175/JCLI-D-17-0168.1>.

Li, H., A. Fedorov, and W. Liu, 2021: AMOC stability and diverging response to arctic sea ice decline in two climate models. *J. Clim.*, **34** (13), 5443–5460, <https://doi.org/10.1175/JCLI-D-20-0572.1>.

Liu, W., S. P. Xie, Z. Liu, and J. Zhu, 2017: Overlooked possibility of a collapsed atlantic meridional overturning circulation in warming climate. *Science Advances*, **3** (1), 1–8, <https://doi.org/10.1126/sciadv.1601666>.

Lobelle, D., F. Sévellec, C. Beaulieu, V. Livina, E. Frajka-williams, D. L. F. S, and B. Valerie, 2022: AMOC Trends From 1850 to 2100 At Interannual To Multi-Decadal Time Scales Corroborated By Changes In Salinity Budget corroborated by changes in salinity budget. *Research Square*, 0–31.

Lozier, M., F. Li, S. Bacon, F. Bahr, A. Bower, and S. e. a. Cunningham, 2019: A sea change in our view of overturning in the subpolar north atlantic. *Science*, **363**, 516?521.

Lozier, M. S., and Coauthors, 2017: Overturning in the Subpolar north Atlantic program: A new international ocean observing system. *Bulletin of the American Meteorological Society*, **98** (4), 737–752, <https://doi.org/10.1175/BAMS-D-16-0057.1>.

Lynch-Stieglitz, J., 2017: The atlantic meridional overturning circulation and abrupt climate change. *Ann. Rev. Mar. Science*, **9**, 83?104.

Manabe, S., and R. Stouffer, 1988: Two stable equilibria of a coupled ocean-atmosphere model. *J. Clim.*, **1**, 841?866.

Manabe, S., and R. J. Stouffer, 1994: Multiple-century response of a coupled ocean-atmosphere model to an increase of atmospheric carbon-dioxide. *Journal of Climate*, **7**, 5–23.

Marshall, J., J. Scott, A. Romanou, M. Kelley, and A. Leboissetier, 2017: The dependence of the ocean's moc on mesoscale eddy diffusivities: A model study. *Ocean Model.*, **111**, <https://doi.org/10.1016/j.ocemod.2017.01.001>.

Masson-Delmotte, V., and Coauthors, Eds., 2021: *Climate Change 2021: The Physical Science Basis. Contribution of Working Group I to the Sixth Assessment Report of the Intergovernmental Panel on Climate Change*. Cambridge University Press.

McCarthy, G. D., D. A. Smeed, W. E. Johns, E. Frajka-Williams, B. I. Moat, and D. e. a. Rayner, 2015: Measuring the atlantic meridional overturning circulation at 26n. *Progr. Oceanogr.*, **130**, 91?111, <https://doi.org/10.1016/j.pocean.2014.10.006>.

Mecking, J. V., S. S. Drijfhout, L. C. Jackson, and M. B. Andrews, 2017: The effect of model bias on Atlantic freshwater transport and implications for AMOC bi-stability. *Tellus, Series A: Dynamic Meteorology and Oceanography*, **69 (1)**, 1–15, <https://doi.org/10.1080/16000870.2017.1299910>, URL <http://dx.doi.org/10.1080/16000870.2017.1299910>.

Mecking, J. V., S. S. Drijfhout, L. C. Jackson, and T. Graham, 2016: Stable AMOC off state in an eddy-permitting coupled climate model. *Clim. Dyn.*, **47 (7-8)**, 2455–2470, <https://doi.org/10.1007/s00382-016-2975-0>.

Meinshausen, M., and Coauthors, 2019: The SSP greenhouse gas concentrations and their extensions to 2500. *Geosci. Mod. Dev. Disc.*, **(October)**, 1–77, <https://doi.org/10.5194/gmd-2019-222>.

Menary, M. B., L. C. Jackson, and M. S. Lozier, 2020: Reconciling the Relationship Between the AMOC and Labrador Sea in OSNAP Observations and Climate Models. *Geophysical Research Letters*, **47 (18)**, <https://doi.org/10.1029/2020GL089793>.

Menary, M. B., and R. A. Wood, 2018: An anatomy of the projected North Atlantic warming hole in CMIP5 models. *Climate Dynamics*, **50 (7-8)**, 3063–3080, <https://doi.org/10.1007/s00382-017-3793-8>.

Men viel, L., A. Timmermann, T. Friedrich, and M. H. England, 2014: Hindcasting the continuum of Dansgaard-Oeschger variability: Mechanisms, patterns and timing. *Climate of the Past*, **10 (1)**, 63–77, <https://doi.org/10.5194/cp-10-63-2014>.

Miller, R. L., and Coauthors, 2021: CMIP6 Historical Simulations (1850?2014) With GISS-E2.1. *J. Adv. Mod. Earth Syst.*, **13 (1)**, 1–35, <https://doi.org/10.1029/2019MS002034>.

- Moffa-Sanchez, P., E. Moreno?Chamarro, D. J. Reynolds, P. Ortega, L. Cunningham, and D. e. a. Swingedouw, 2019: Variability in the northern north atlantic and arctic oceans across the last two millennia: A review. *Paleoceanography and Paleoclimatology*, **34** (8), 1399?1436, <https://doi.org/doi.org/10.1029/2018PA003508>.
- Nazarenko, L. S., and co authors, 2022: Future climate change under ssp emission scenarios with giss-e2.1. *J. Adv. Mod. Earth Syst.*, <https://doi.org/10.1029/2019MS002034>.
- Petit, T., M. S. Lozier, S. A. Josey, and S. A. Cunningham, 2020: Atlantic deep water formation occurs primarily in the iceland basin and irminger sea by local buoyancy forcing. *Geophys. Res. Lett.*, **47**, <https://doi.org/doi.org/10.1029/2020gl091028>.
- Pickart, R. S., and M. A. Spall, 2007: Impact of labrador sea convection on the north atlantic meridional overturning circulation. *J. Phys. Oceanogr.*, **37**, 2207?2227.
- Prather, M. J., 1986: Numerical advection by conservation of second order moments. *J. Geophys. Res.*, **91**, 6671–6680.
- Rahmstorf, S., 1996: On the freshwater forcing and transport of the Atlantic thermohaline circulation. *Clim. Dyn.*, **12** (12), 799–811, <https://doi.org/10.1007/s003820050144>.
- Ren, L., and S. C. Riser, 2009: Seasonal salt budget in the northeast Pacific Ocean. *J. Geophys. Res.: Oceans*, **114** (12), 1–11, <https://doi.org/10.1029/2009JC005307>.
- Rhein, M., and Coauthors, 2011: Deep water formation, the subpolar gyre, and the meridional overturning circulation in the subpolar north atlantic. *Deep Sea Res., Part II*, **58**, 1819?1832, <https://doi.org/10.1016/j.dsr2.2010.10.061>.
- Rind, D., P. Demenocal, G. L. Russell, S. Sheth, D. Collins, G. A. Schmidt, and J. Teller, 2001: Effects of glacial meltwater in the GISS Coupled Atmosphere-Ocean Model: Part I: North Atlantic Deep Water response. *J. Geophys. Res.*, **106**, 27,335–27,354.
- Rind, D., G. A. Schmidt, J. Jonas, R. L. Miller, L. Nazarenko, M. Kelley, and J. Romanski, 2018: Multi-century instability of the atlantic meridional circulation in rapid warming simulations with giss modele2. *J. Geophys. Res. Atmos.*, **123** (12), 6331–6355, <https://doi.org/10.1029/2017JD027149>.

- Romanou, A., J. Marshall, M. Kelley, and J. Scott, 2017: Role of the ocean's amoc in setting the uptake efficiency of transient tracers. *Geophys. Res. Lett.*, **44**, 5590–5598, <https://doi.org/10.1002/2017gl072972>.
- Rooth, C., 1982: Hydrology and ocean circulation. *Progr. Oceanogr.*, **11 (2)**, 131?149.
- Russell, G., J. Miller, and D. Rind, 1995: A coupled atmosphere?ocean model for transient climate change studies. *Atmos. Ocean*, **33**, 683?730.
- Schmidt, G. A., C. M. Bitz, U. Mikolajewicz, and L. B. Tremblay, 2004: Ice-ocean boundary conditions for coupled models. *Ocean Model.*, **7**, 59–74.
- Schmidt, G. A., and A. N. LeGrande, 2005: The goldilocks abrupt climate change event. *Quat. Sci. Rev.*, **24**, 1109–1110, <https://doi.org/10.1016/j.quascirev.2005.01.015>.
- Schott, F., L. Stramma, B. Giese, and R. Zantopp, 2009: Labrador sea convection and subpolar north atlantic deep water export in the soda assimilation model. *Deep Sea Res.*, **56**, 926?938, <https://doi.org/10.1016/j.dsr.2009.01.001>.
- Sgubin, G., D. Swingedouw, S. Drijfhout, S. Hagemann, and E. Robertson, 2015: Multimodel analysis on the response of the AMOC under an increase of radiative forcing and its symmetrical reversal. *Climate Dynamics*, **45 (5-6)**, 1429–1450, <https://doi.org/10.1007/s00382-014-2391-2>, URL <http://dx.doi.org/10.1007/s00382-014-2391-2>.
- Sgubin, G., D. Swingedouw, S. Drijfhout, Y. Mary, and A. Bennabi, 2017: Abrupt cooling over the North Atlantic in modern climate models. *Nature Comm.*, **8**, <https://doi.org/10.1038/ncomms14375>.
- Sijp, W., M. England, and J. Gregory, 2012: Precise calculations of the existence of multiple amoc equilibria in coupled climate models. part i: equilibrium states. *J. Clim.*, **25**, 282?298.
- Spall, M. A., 2004: Boundary currents and watermass transformation in marginal seas. *J. Phys. Oceanogr.*, **34**, 1197?1213, [https://doi.org/doi.org/10.1175/1520-0485\(2004\)034<1197:bcawti>2.0.co;2](https://doi.org/doi.org/10.1175/1520-0485(2004)034<1197:bcawti>2.0.co;2).
- Stocker, T., Q. Dahe, and G.-K. Plattner, Eds., 2013: *Climate Change 2013: The Physical Science Basis. Contribution of Working Group I to the Fifth Assessment Report of the Intergovernmental*

Panel on Climate Change. Cambridge University Press, Cambridge, United Kingdom and New York, NY, USA.

Stommel, H., 1961: Thermohaline convection with two stable regimes of flow. *Tellus*, **13**, 224?230.

Stouffer, R., and Coauthors, 2006: Investigating the causes of the response of the thermohaline circulation to past and future climate changes. *J. Clim.*, **19**, 1365?1387, <https://doi.org/doi.org/10.1175/JCLI3689.1>.

Swingedouw, D., A. Bily, C. Esquerdo, L. F. Borchert, G. Sgubin, J. Mignot, and M. Menary, 2021: On the risk of abrupt changes in the North Atlantic subpolar gyre in CMIP6 models. *Annals of the New York Academy of Sciences*, **1504** (1), 187–201, <https://doi.org/10.1111/nyas.14659>.

Swingedouw, D., P. Braconnot, P. Delecluse, E. Guilyardi, and O. Marti, 2007: Quantifying the amoc feedbacks during a 2xco₂ stabilization experiment with land-ice melting. *Clim Dyn*, **29**, 521–534, <https://doi.org/10.1007/s00382-007-0250-0>.

Talley, L. D., J. L. Reid, and P. E. Robbins, 2003: Data-based meridional overturning streamfunctions for the global ocean. *J. Clim.*, **16**, 3213?3226, [https://doi.org/10.1175/1520-0442\(2003\)016<3213:DMOSFT>2.0.CO;2](https://doi.org/10.1175/1520-0442(2003)016<3213:DMOSFT>2.0.CO;2).

Thomas, M. D., and A. V. Fedorov, 2019: Mechanisms and Impacts of a Partial AMOC Recovery Under Enhanced Freshwater Forcing. *Geophysical Research Letters*, **46** (6), 3308–3316, <https://doi.org/10.1029/2018GL080442>.

Thornalley, D. J., and Coauthors, 2018: Anomalously weak Labrador Sea convection and Atlantic overturning during the past 150 years. *Nature*, **556** (7700), 227–230, <https://doi.org/10.1038/s41586-018-0007-4>.

Trenberth, K. E., and A. Solomon, 1994: The global heat-balance: Heat transports in the atmosphere and ocean. *Clim. Dyn.*, **10**, 107–134, <https://doi.org/10.1007/BF00210625>.

Weaver, A. J., and Coauthors, 2012: Stability of the Atlantic meridional overturning circulation: A model intercomparison. *Geophysical Research Letters*, **39** (20), 1–8, <https://doi.org/10.1029/2012GL053763>.

Weber, S. L., and Coauthors, 2007: The modern and glacial overturning circulation in the Atlantic ocean in PMIP coupled model simulations. *Climate of the Past*, **3** (1), 51–64, <https://doi.org/10.5194/cp-3-51-2007>.

Weijer, W., W. Cheng, O. A. Garuba, A. Hu, and B. T. Nadiga, 2020: CMIP6 Models Predict Significant 21st Century Decline of the Atlantic Meridional Overturning Circulation. *Geophys. Res. Lett.*, **47** (12), <https://doi.org/10.1029/2019GL086075>.

Weijer, W., and Coauthors, 2019: Stability of the Atlantic Meridional Overturning Circulation: A Review and Synthesis. *J. Geophys. Res.: Oceans*, **124** (8), 5336–5375, <https://doi.org/10.1029/2019JC015083>.

Yashayaev, I., and J. Loder, 2009: Enhanced production of labrador sea water in 2008. *Geophys. Res. Lett.*, <https://doi.org/10.1029/2008gl036162>.

Zhang, J., and D. Rothrock, 2000: Modeling Arctic sea ice with an efficient plastic solution. *J. Geophys. Res.*, **105**, 3325–3338.

Zhang, X., G. Knorr, G. Lohmann, and S. Barker, 2017: Abrupt North Atlantic circulation changes in response to gradual CO₂ forcing in a glacial climate state. *Nature Geoscience*, **10** (7), 518–523, <https://doi.org/10.1038/ngeo2974>.

Zou, S., M. S. Lozier, and M. Buckley, 2019: How Is Meridional Coherence Maintained in the Lower Limb of the Atlantic Meridional Overturning Circulation? *Geophys. Res. Lett.*, **46** (1), 244–252, <https://doi.org/10.1029/2018GL080958>.